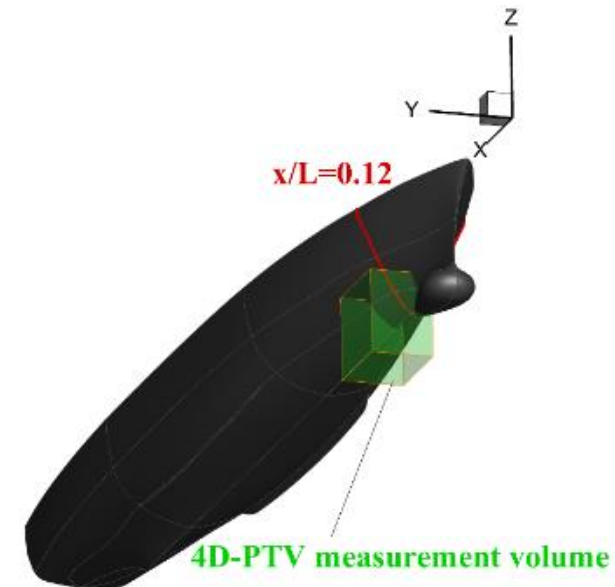


4DPTV Measurements and DES of the Turbulence Structure and Vortex Breakdown and Interaction for 5415 Sonar Dome

Frederick Stern¹, Yugo Sanada¹, Zachary Starman¹, Shanti Bhushan², Christian Milano¹
(¹IIHR, University of Iowa, USA, ²Mississippi State University, USA)

1. Introduction
2. Experimental and DES Methods
3. Macro Features and Large Scales
4. Spectral Analysis and Small Scales
5. Turbulence Anisotropy
6. Vortex Breakdown and Interaction
7. Conclusions and Future Research

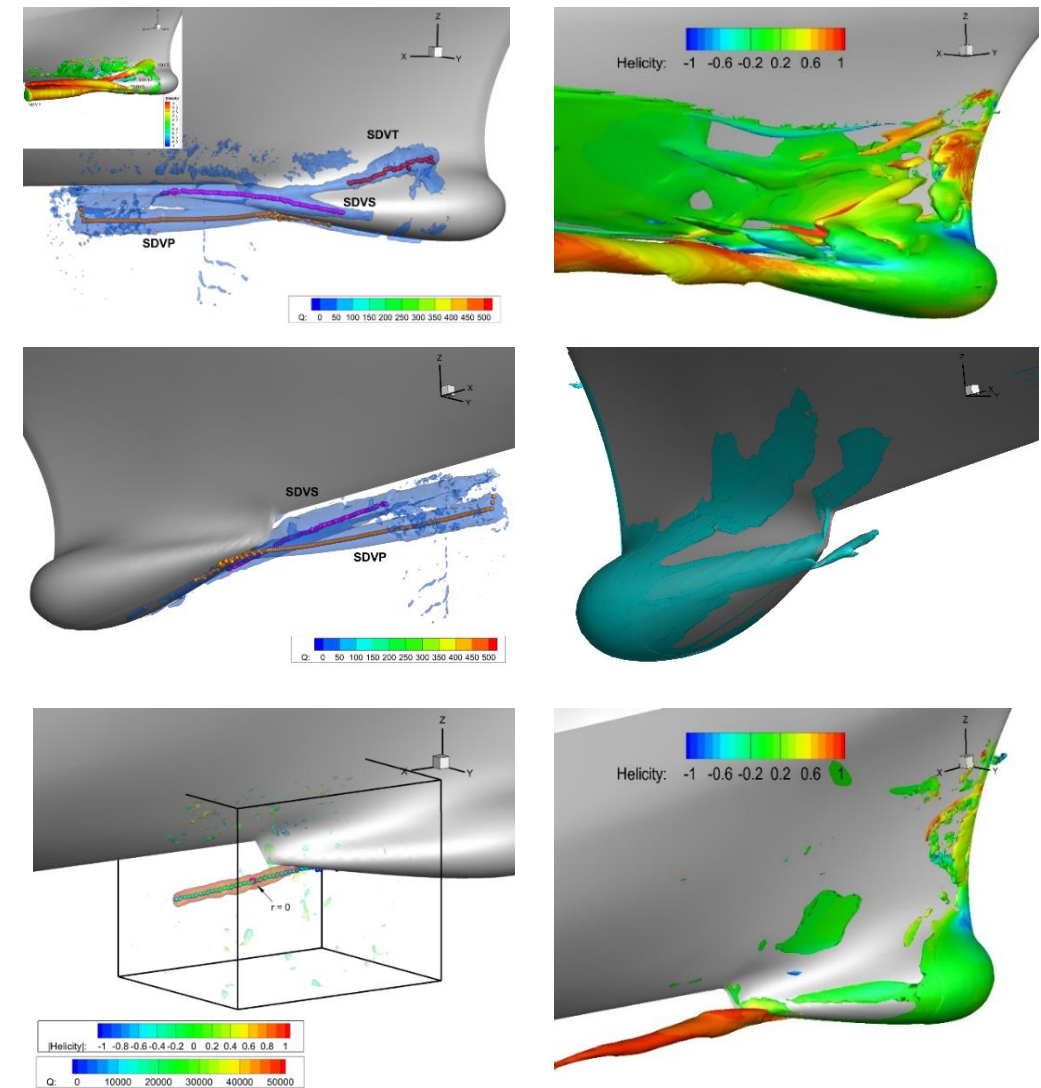


4DPTV measurement volume for SDVP vortex core at $x/L = 0.12$.

Acknowledgements: This research was sponsored by the Office of Naval Research under grants N00014-21-1-2060 and N00014-21-1-2399 under the administration of Dr. Woei-Min Lin.

Introduction

- The physics, measurement, and prediction of 3D vortex onset and progression, including turbulence structure and vortex breakdown and interactions remains an ongoing fluid dynamics challenge.
- Previous work of Sanada et al. (2023) showed significant progress on physics of the 3D vortex onset and progression for the 5415 sonar dome vortices via Four-dimensional particle tracking velocimetry (4DPTV) due to its significantly larger measurement volume and data rate in comparison to previous tomographic particle image velocimetry (TPIV) measurements (Yoon and Stern, 2017; Bhushan et al., 2019 and 2021).
- The objective of the present research is the additional analysis of the 4DPTV static drift $\beta = 10$ deg results to realize its full potential for:
 1. Assessing the turbulence structure and vortex breakdown and interactions
 2. Providing data for scale resolved CFD validation
 3. Identify its limitations for future advancements in instrumentation.
- The current analysis is subject to the 4DPTV $\{2 - 4\}$ mm spatial resolution. Part of this research is focused on understanding the limitations of this method and evaluating future improvements, e.g., the acquisition of a new lens enabling 1 mm spatial resolution.



SDVP, SDVS, SDVT, and SDVT2 vortices (top and middle) and turbulence analysis location for SDVP core (bottom).

Experimental and DES Methods

Experimental Methods

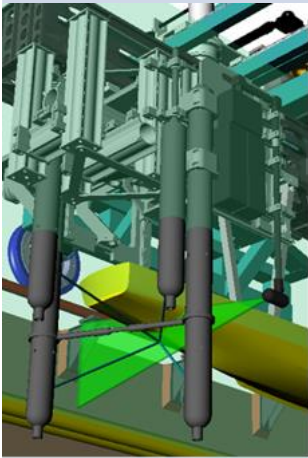
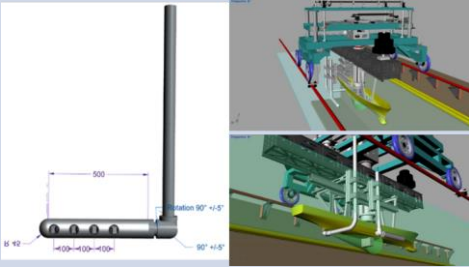
- Sanada, Y., Starman, Z., Bhushan, S., and Stern, F., “Four-dimensional particle tracking velocimetry measurements of unsteady 3D vortex onset and progress for 5415 straight ahead, static drift and pure sway,” *Physics of Fluids*, Vol. 35(10), 2023, 105125. <https://doi.org/10.1063/5.0165658>.

Advantages of 4DPTV

- Data rate: 444.2 Hz (TPIV: 15 Hz)
- Measurement Volume: 200 m³ (20 times larger than TPIV)
- No strong laser specular reflections on the hull surface. There is no black area like SPIV/TPIV.

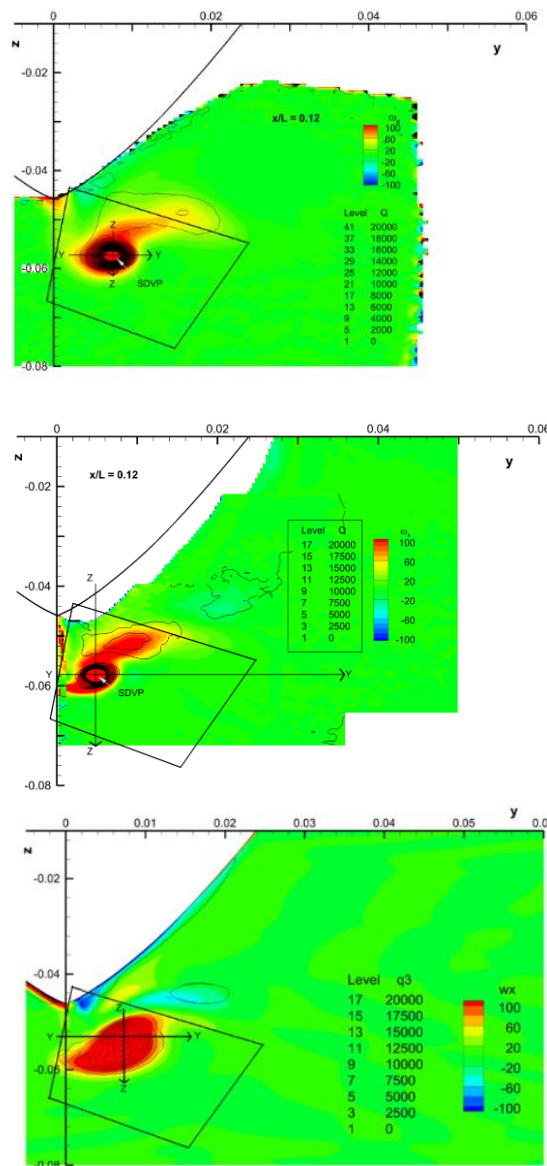
DES Methods

- Bhushan, S., Yoon, H., and Stern, F., “Detached Eddy Simulations and Tomographic PIV Measurements of Flows over Surface Combatant 5415 at Straight-Ahead and Static Drift Conditions,” *Ocean Engineering*, Vol. 238, 2021, 109658.

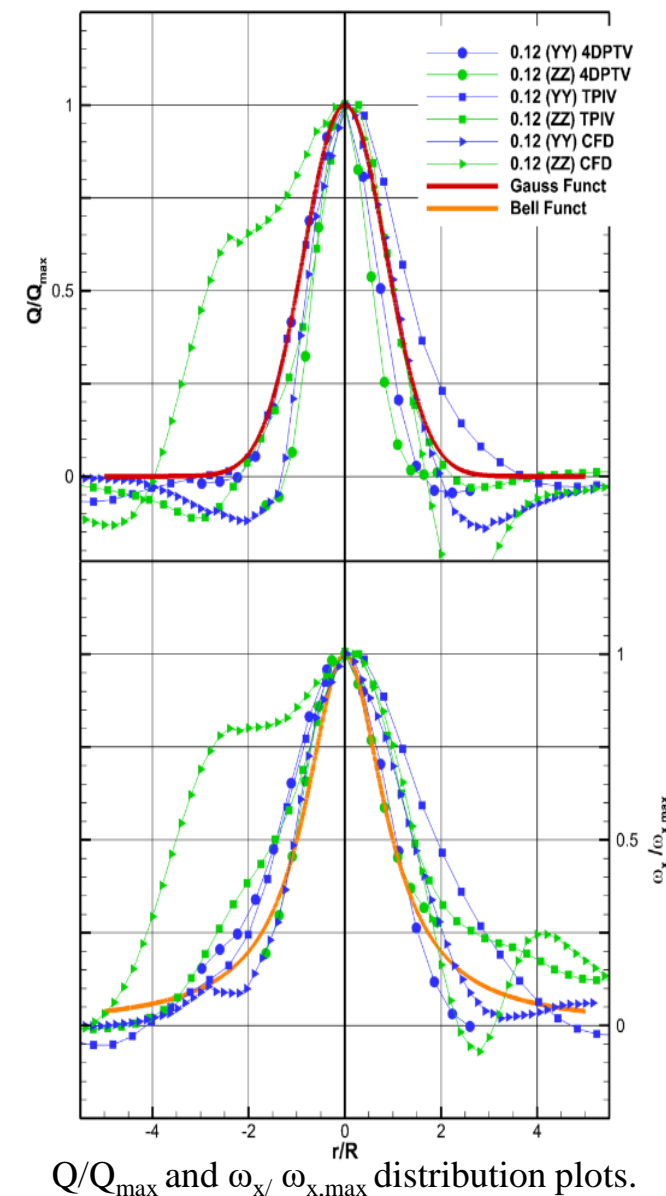
	TPIV	4DPTV
Number of Cameras	4	4
Frame rate	15 fps (Up to 28)	444 fps (Up to 600)
Lasing medium	Nd:YAG	Nd:YLF
Repetition rate	Up to 15 Hz	Up to 10 kHz
Measurement Area/Volume size	100 mm × 100 mm × 15 mm	200 mm × 150 mm × 100 mm
Spatial Resolution	1 mm	2.1 mm or 4.2 mm (Current setup)
System Drawing		

Macro Features and Large Scales (1)

- TPIV and 4DPTV results are similar with both indicating elliptically shaped cross plane streamlines and substantial interactions between the SDVP and the other vortices, especially SDVS. The DES is similar but clearly less resolved than both experiments.
- Comparisons of the 4DPTV and TPIV normalized Q/Q_{max} and mean axial vorticity $\omega_x/\omega_{x,max}$ vs. r/R for horizontal YY and vertical ZZ cuts through the vortex core with Gaussian and Bell distributions show close agreement, respectively.
 - Gaussian: $f(r) = e^{-\left(\frac{5r}{3W}\right)^2}$
 - Bell: $f(r) = \left(1 + \left|\frac{2r}{w}\right|^2\right)^{-1}$
- DES shows less agreement with the distribution than the experiments, especially for the ZZ cut in negative direction. The reason for the differences in the ZZ cut is a secondary peak for the DES, which is attributed to its larger diffusion and increased interactions between the SDVP and SDVS vortices than that shown by the experiments.
- Vortex width is estimated by the criteria: $R = W/2$ at $Q/Q_{max} = 0.5$, where W is the half-width of the vortex.



Axial vorticity (ω_x) contour with Q isolines of 4DPTV (top), TPIV (middle), and DES (bottom).



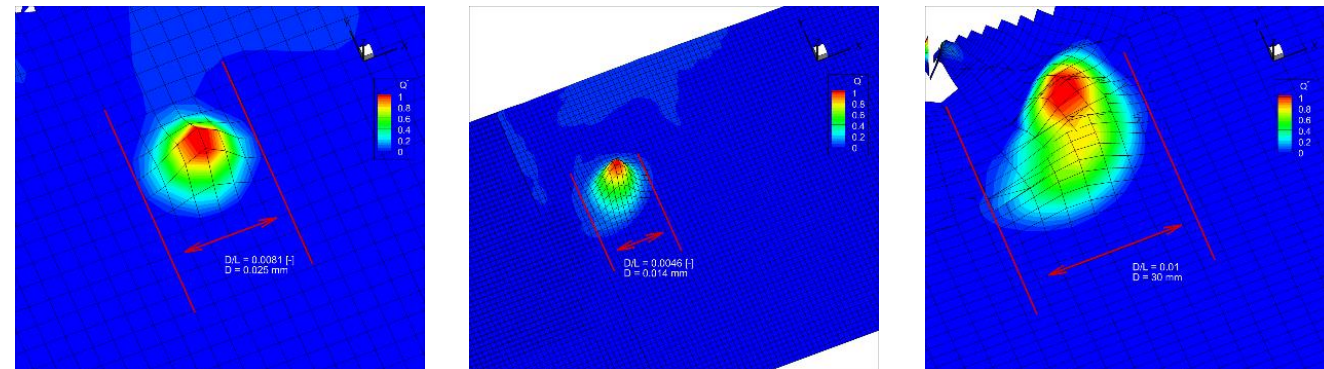
Q/Q_{max} and $\omega_x/\omega_{x,max}$ distribution plots.

Macro Features and Large Scales (2)

- The core locations and R values for the experiments show similar trends; however, the TPIV core location is closer to the center plane, somewhat deeper, and average R is 23% smaller than the 4DPTV.
- The DES core location and size are closer to the 4DPTV than the TPIV; nonetheless, nearly 40% larger than the 4DPTV and 80% larger than the TPIV.
- The 3D contour of Q for the 4DPTV and TPIV indicate that the vortex patterns are nearly symmetric, whereas the DES is asymmetric.
- The 4 mm 4DPTV has less points within the vortex than the 2 mm resolution (not shown) and the TPIV and DES.
- Based on these figures, the estimate of the vortex diameter, based on the Q contour level of zero, is approximately $l_0 = 25$ mm for the 4DPTV. In comparison, it is 14 mm for the TPIV and 30 mm for the DES.

Measurement	Core		$R = \frac{W}{2}$ at $\frac{Q}{Q_{\max}} = 0.5$			
	y [-]	z [-]	YY [-]	ZZ [-]	Mean [-]	Mean [m]
4DPTV (2mm)	0.0076	-0.0573	0.0014	0.0015	0.0015	0.0045
TPIV	0.0048	-0.0577	0.0011	0.0011	0.0011	0.0034
TPIV % 4DPTV	36.84%	-0.70%	22.54%	24.00%	23.29%	23.29%
DES	0.0071	-0.0527	0.0020	0.0020	0.0020	0.0061
DES % 4DPTV	6.58%	8.03%	-40.85%	-33.33%	-36.99%	-36.99%
DES % TPIV	-47.92%	8.67%	-81.82%	-75.44%	-78.57%	-78.57%

Core Location and Vortex Width Based on Cutline Distribution.



Q/Q_{\max} 3D Contour with Mesh for 4DPTV 4mm (left), TPIV (middle), and DES (right).

Macro Features and Large Scales (3)

- **4DPTV**

- Mean velocity $\langle U \rangle$ is $0.80U$.
- The turbulent velocity scale $u_0 = \sqrt{k}$ is 17.4% of the mean velocity $\langle U \rangle$.
- Turbulent length scale $L = \frac{l_0}{0.43}$, $Re_L = \frac{\sqrt{k}L}{\nu} = 10780$
- The dissipation $\varepsilon = u_0^3/l_0 = 0.181 \text{ m}^2/\text{s}^3$.

- **TPIV**

- 14% smaller $\langle U \rangle$.
- 35% smaller $\langle u^2 \rangle$ and k such that u_0 is 21% smaller.
- Since l_0 is 44% smaller, ε is 12% smaller.
- The resulting Re_L is 55.7% smaller than the 4DPTV.

Parameter	4DPTV	TPIV	TPIV % 4DTPV	DES	DES % 4DPTV	DES % TPIV
$\langle U \rangle$ [m/s]	1.255	1.081	-13.86%	1.313	4.62%	21.46%
$\langle u^2 \rangle$ [m ² /s ²]	0.018	0.012	-33.33%	0.002	-88.89%	-83.33%
k [m ² /s ²]	0.048	0.030	-37.50%	0.014	-70.83%	-53.33%
u_0 [m/s]	0.219	0.173	-21.00%	0.095	-56.62%	-45.09%
l_0 [m]	0.025	0.014	-44.00%	0.030	20.00%	114.29%
ε [m ² /s ³]	0.181	0.160	-11.60%	0.012	-93.37%	-92.50%
Re_L	10780	4771	-55.74%	5601	-48.04%	17.40%

Macro-scale vortex core parameters.

- The turbulence is much stronger for 4DPTV vs. TPIV measurements, and both are stronger than the DES.

- 4DPTV and TPIV indicate similar anisotropy of the turbulence: $\frac{3}{2}\langle u^2 \rangle \sim \begin{cases} 0.56 & \text{4DPTV} \\ 0.60 & \text{TPIV} \\ 0.29 & \text{DES} \end{cases} \rightarrow \langle v^2 \rangle$ and $\langle w^2 \rangle$ are much larger than $\langle u^2 \rangle$.

- **DES**

- Shows better agreement with the 4DPTV for $\langle U \rangle$ and l_0 , whereas it shows better agreement with the TPIV for k , u_0 , and Re_L ; the dissipation ε shows large error with both the 4DPTV and TPIV.

Macro Features and Large Scales (4)

- Time mean circulation $\langle \Gamma \rangle$, normalized time mean circulation $\langle \Gamma \rangle / \langle U \rangle l_0$, time mean tangential velocity of the vortex core $\langle U_\theta \rangle$ and corresponding swirl number $S = \langle U_\theta \rangle / \langle U \rangle$ evaluated based on Stokes theorem:

$$\langle \Gamma \rangle = \oint_C \langle \mathbf{U} \rangle \cdot d\mathbf{r} = \int_A \langle \boldsymbol{\Omega} \rangle \cdot \mathbf{n} dA = \int_A \Omega_x dA$$

- $\langle U_\theta \rangle$ is obtained by dividing $\langle \Gamma \rangle$ by the perimeter of line integral:

$$\langle U_\theta \rangle = \langle \Gamma \rangle / L_{\text{perimeter}}$$

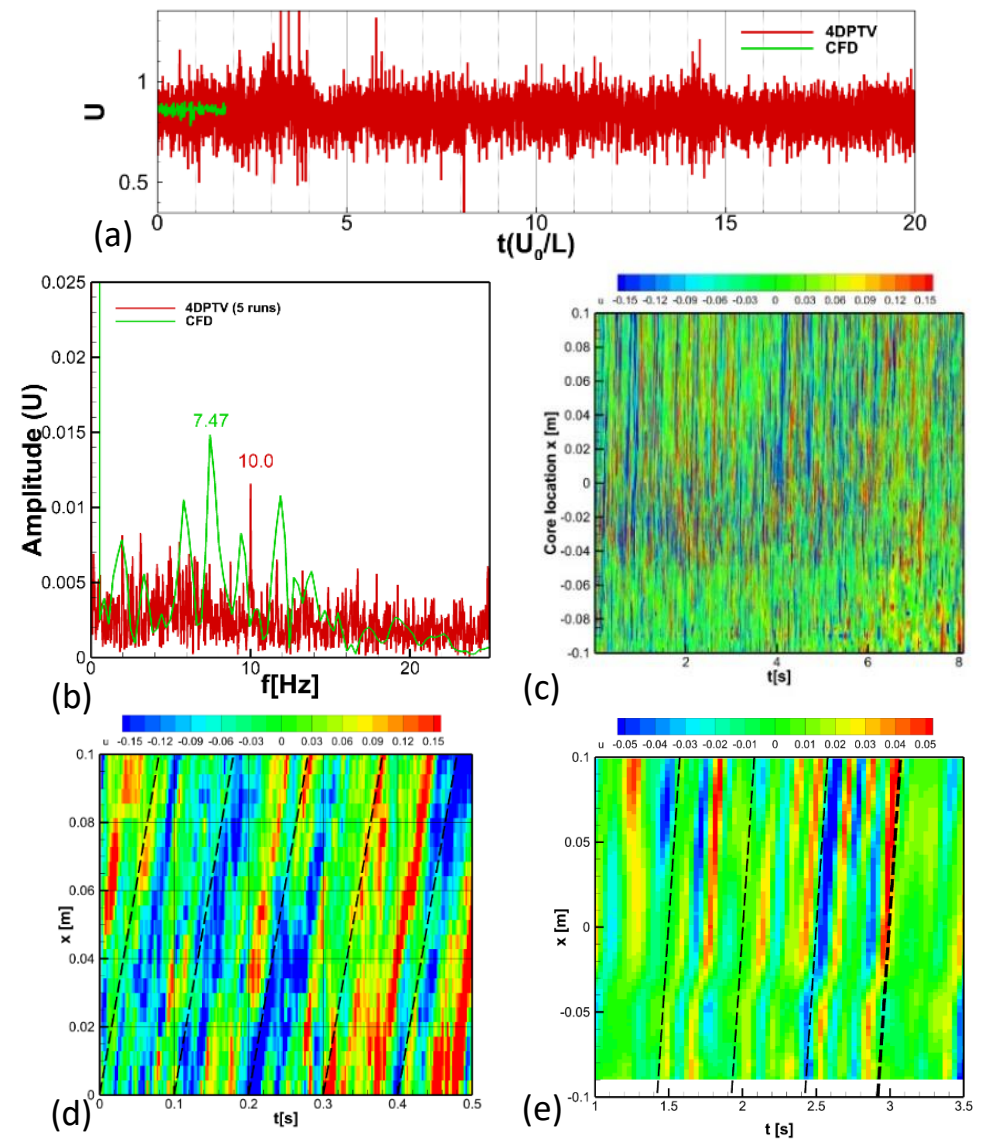
Parameter	4DPTV	TPIV	TPIV % 4DTPV	DES	DES % 4DPTV	DES % TPIV
$\langle \Gamma \rangle [m^2/s]$	0.0302	0.0226	25.18%	0.0341	-12.69%	-50.61%
$\frac{\langle \Gamma \rangle}{\langle U \rangle l_0} [-]$	0.9683	1.4650	-51.30%	0.8808	9.03%	39.88%
$\langle U_\theta \rangle [m/s]$	0.3533	0.3748	-6.09%	0.2229	36.90%	40.52%
$\frac{\langle U_\theta \rangle}{U} [-]$	0.2308	0.2448	-6.09%	0.1456	36.90%	40.52%
$S = \frac{\langle U_\theta \rangle}{\langle U \rangle} [-]$	0.2829	0.3398	-20.11%	0.1740	38.49%	48.79%

Vortex Circulation and Swirl Number.

- 4DPTV dimensional $\langle \Gamma \rangle$ larger than TPIV, whereas the non-dimensional $\langle \Gamma \rangle / \langle U \rangle l_0$ is smaller.
- The swirl numbers are smaller for the 4DPTV vs. TPIV. Thus, the vortex strength is larger for TPIV vs. 4DPTV. DES shows better agreement with 4DPTV than TPIV, but with large errors.
- The swirl numbers are all much less than the critical values provided in the literature for vortex breakdown for wing tip ($Sc \approx 2 - 3$) and delta wing ($Sc \approx 1$) vortices. Nonetheless, as shown in Sanada et al. (2023), SDVP undergoes vortex breakdown, which is attributed to vortex-vortex interactions.
- It is not possible to say with confidence, which is more accurate, as TPIV has somewhat higher spatial resolution, whereas 4DPTV has much higher temporal resolution and lower uncertainties.

Spectral Analysis and Small Scales

- The 1D axial velocity $u(t)$ spectral analysis and evaluation of the small scales is done using both temporal and spatial (along the time mean vortex core) autocorrelations and energy spectrums. 3D energy spectrums are also obtained from the 1D energy spectrums using isotropic tensor theory.
- Preliminary to the analysis of the axial velocity energy spectrum, an analysis is made of its time series along the SDVP vortex core upstream and downstream of $x/L = 0.12$ and its FFT at $x/L = 0.12$.
- A dominant frequency is clearly observed at frequencies 10.0 and 7.47 Hz [Strouhal numbers ($St = fL/U$) are 19.9 and 14.9, respectively] for the 4DPTV and DES, respectively.
- Figure (c) shows the $u(x, t)$ contours upstream and downstream of $x/L = 0.12$ for $-0.03 \leq x/L \leq 0.03$ and $0 \leq t \leq 8$ s; and Figures (d,e) show zoomed in views for $-0.03 \leq x/L \leq 0.03$ and $0 \leq t \leq 0.5$ s.
- The temporal oscillations for the 4DPTV and DES are shown to occur at periods of approximately 0.1 and 0.13 s, respectively, which correspond to frequencies 10 and 7.47 Hz and are attributed to the spiral vortex breakdown/helical mode instability.
- Figures (d,e) also clearly shows the existence of $u(x, t)$ spatial waves traveling in the positive x direction. The wave speed dx/dt is estimated for the 4DPTV and DES to be 1.25 and 1.33 m/s, which coincides with their estimated mean vortex core velocities.
- The turbulence is transported by the mean velocity, which supports the later use of the Taylor hypothesis. The spatial waves are also due to the spiral vortex breakdown/helical mode instability with wavelengths λ estimated at $x/L = 0.12$ based on the wave speed times the wave period, i.e., $\lambda = 0.125$ and 0.133 m for the 4DPTV and DES, respectively.



$u(t)$ at SDVP core: time series (a) and FFT analysis (b) at $x/L = 0.12$ (b); $u(t)$ vs. time and space upstream and downstream of $x/L = 0.12$ (c,d,e).

- Temporal analysis:
 - DES only for power spectral density approach.
 - 4DPTV for both temporal autocorrelation and power spectral density approaches with same results.
- 4DPTV temporal minimum and maximum ranges correspond to the data rate and duration (restricted by towing tank length) of 8s.
- 4DPTV spatial minimum and maximum ranges correspond to the minimum and maximum spatial resolutions.
- DES time-step of $dt = 0.002L/U = 0.00398$ s. However, simulation results are written at every fourth time-step and after resampling $dt = 0.008L/U = 0.0159$ s. The data acquisition time interval of the DES is approximately 3.6s.

	Analysis Type		Resolution		$\omega_{\min}(\text{d}\omega)$ [Hz]	ω_{\max} [Hz]	$\kappa_{1\min}$ [m^{-1}]	$\kappa_{1\max}$ [m^{-1}]	$l_{1\min}$ [m]	$l_{1\max}$ [m]
4DPTV	Temporal		dt	2.25E-03	1.23E-01	2.22E+02	6.18E-01	1.11E+03	6.00E-03	1.02E+01
	Space	Symmetric	dx	4.277E-03			2.83E+01	7.34E+02	9.00E-03	2.22E-01
		Antisymmetric	dx	4.277E-03			2.83E+01	7.34E+02	9.00E-03	2.22E-01
		Direct ε	dx	4.277E-03			2.83E+01	7.34E+02	9.00E-03	2.22E-01
DES	Temporal	Time	dt	1.59E-02			2.78E-01	3.11E+01	1.33E+00	1.48E+02

4DPTV and DES resolution, frequency limitations, and length scales.

- 3D model spectrum defined as per Pope (2000):

$$E(k) = C\varepsilon^{\frac{2}{3}}k^{-\frac{5}{3}}f_L(kL)f_\eta(k\eta)$$

$$f_\eta(k\eta) = \exp\left\{-\beta\left\{\left[(k\eta)^4 + c_\eta^4\right]^{\frac{1}{4}} - c_\eta\right\}\right\}$$

$$f_L(kL) = \left(\frac{kL}{[(kL)^2 + c_L]^{\frac{1}{2}}}\right)^{\frac{5}{3} + p_0}$$

- $L, k,$ and ν given by macro-scale vortex parameters, while c_L and c_η selected such that:

$$\int_0^\infty E(\kappa)d\kappa = k_{BM} \quad \int_0^\infty 2\nu\kappa^2 E(\kappa)d\kappa = \varepsilon_{BM}$$

- $C=1.5, \beta=5.2, p_0=2, c_L=5.76, c_\eta=0.40$ for both TPIV and 4DPTV.
- 1D model energy spectrum $E_{11}(k_1)$ can be obtained from 3D model spectrum $E(k)$ and vice versa:

$$E_{11}(\kappa_1) = \int_{\kappa_1}^\infty \frac{E(\kappa)}{\kappa} \left(1 - \frac{\kappa_1^2}{\kappa^2}\right) d\kappa$$

$$E(k) = \frac{1}{2}k^3 \frac{d}{dk} \left(\frac{1}{k} \frac{dE_{11}(\kappa)}{d\kappa}\right)$$

- Based on the model spectrum and the scaling estimates, a set of benchmark comparison values was generated:

- $\lambda_f = \sqrt{20}LRe_L^{-1/2}$

- $\lambda_g = \lambda_f/\sqrt{2}$

They represent a measure of the size of flow features where the viscous effects are important, i.e., the smallest scales of turbulence.

- Re_L obtained from macro scale

- $\Lambda_f = L_{11}$

- $R_\lambda = k^{1/2}\lambda_g/\nu$ (k from macro scale and $\lambda_g = \lambda_f/\sqrt{2}$ from above)

- $\varepsilon = \frac{30\nu\langle u^2 \rangle}{\lambda_f^2}$ ($\langle u^2 \rangle$ from macro scale and $\lambda_f = \sqrt{20}LRe_L^{-1/2}$)

- $\eta = \left(\frac{\nu^3}{\varepsilon}\right)^{1/4}$ (Using micro scale ε)

- Temporal autocorrelation function:

$$R_E(\tau) = \frac{\langle u(t)u(t+\tau) \rangle}{\langle u^2 \rangle}$$

- Fourier transform of $R_E(\tau)$:

$$\hat{R}_E(2\pi\omega) = 2 \int_0^\infty R_E(\tau) \cos(2\pi\omega\tau) d\tau$$

- Temporal micro (τ_E) and macro (T) scales:

$$\tau_E = \left[\frac{-2}{R_E''(0)} \right]^{1/2} \quad T = \int_0^\infty R_E(\tau) d\tau$$

- Taylor micro (λ_f) and macro (Λ_f) length scales calculated using Taylor hypothesis:

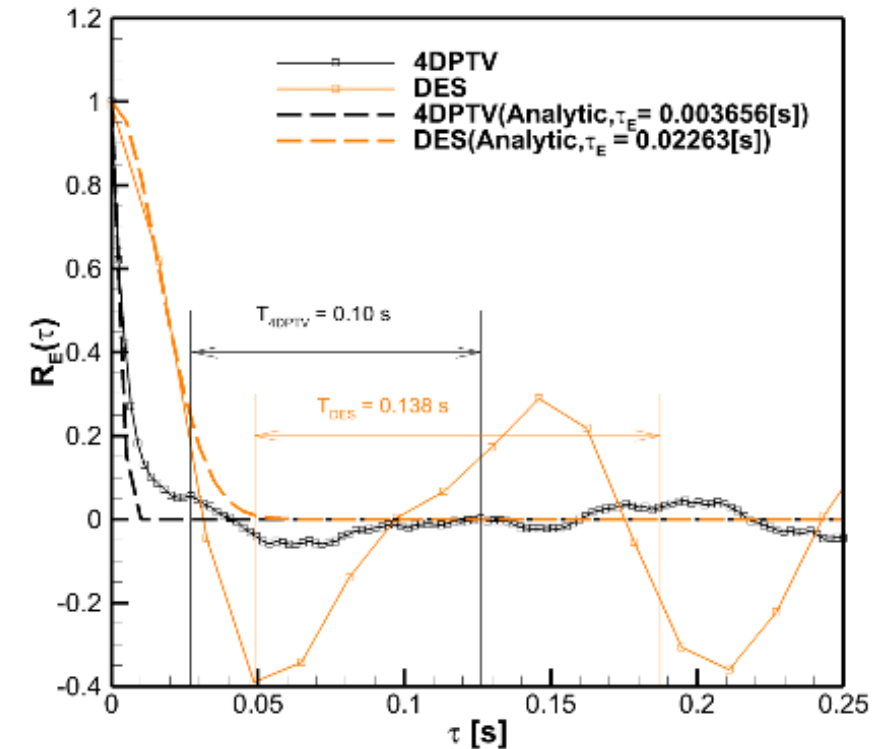
$$\lambda_f = \bar{U}\tau_E \quad \Lambda_f = \bar{U}T$$

- Resulting dissipation (ε) and Kolmogorov length scale (η) are:

$$\varepsilon = \frac{30\nu\langle u^2 \rangle}{\lambda_f^2} \quad \eta = \left(\frac{\nu^3}{\varepsilon} \right)^{1/4}$$

- Both the 4DPTV and DES temporal autocorrelations exhibit the anticipated Gaussian profile for small values of τ . Additionally, they display oscillations for τ greater than approximately 0.02 s and 0.03 s, respectively. The periods of the 4DPTV and DES oscillations are 0.1 s and 0.138 s, respectively, which correspond to the peaks shown in the $u(x, t)$ FFT and its 1D energy spectrum and are attributed to the spiral vortex breakdown/helical mode instability.

- These observations align closely with the analytical solution of the dissipation range, $\exp(-t^2/\tau_E^2)$, for τ values preceding the onset of the oscillations.



Longitudinal autocorrelation: temporal with analytic function $R_E(\tau) = e^{-\tau^2/\tau_E^2}$.

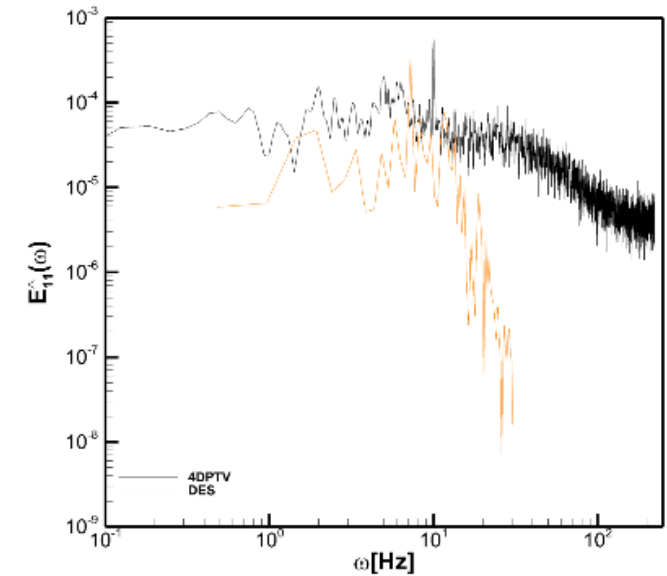
Spectral Analysis and Small Scales: Temporal Spectrum (2)

- 1D energy spectrum in time and space:

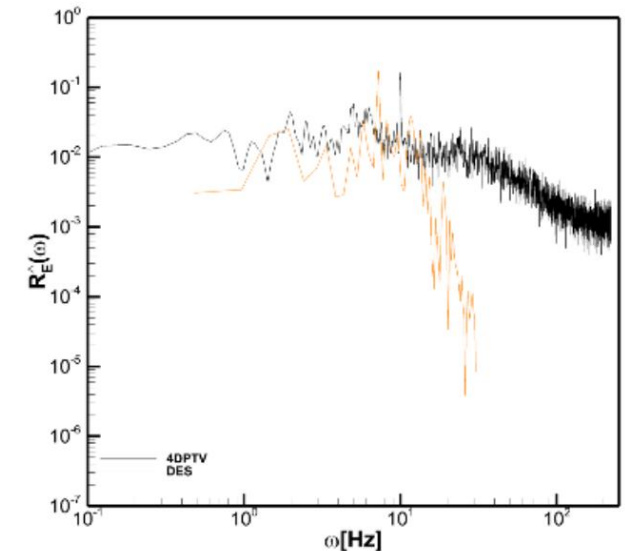
$$\hat{E}_{11}(\omega) = 2\langle u^2 \rangle \hat{R}_E(2\pi\omega) = \lim_{T \rightarrow \infty} \frac{1}{T} |\hat{u}(\omega)|^2$$

$$E_{11}(k_1) = \frac{\bar{U}}{2\pi} \hat{E}_{11}(\omega)$$

- The 4DPTV and DES $\hat{R}_E(2\pi\omega)$ and $\hat{E}_{11}(\omega)$ show similar trends for $\omega < 15$ Hz, although the DES magnitudes are somewhat and significantly smaller, and in both cases clearly less resolved.
- The larger differences for $\hat{E}_{11}(\omega)$ than $\hat{R}_E(2\pi\omega)$ are due to the differences in their scaling and the much larger $\langle u^2 \rangle$ for the 4DPTV vs. the DES.
- The 4DPTV and DES show clear peaks around 10 and 7.47 Hz, respectively.
- For $\omega > 15$ Hz, the 4DPTV shows gradual dissipation, whereas the DES shows rapid dissipation and much less resolution. The frequency resolution of DES is degraded compared to 4DPTV because of the duration of DES time series data being shorter than that of the 4DPTV.
- A longer duration and/or a finer time step of the DES data set is required to improve the frequency resolution. A finer grid would also improve the resolution.



Temporal autocorrelation: temporal 1D energy spectrum.



Temporal autocorrelation: Fourier transform.

- **Symmetric spatial autocorrelation function:**

$$f(r) = \frac{\langle u(x)u(x+r) \rangle}{\langle u^2 \rangle}$$

- Fourier transform of $f(r)$ gives $E_{11}(k_1)$:

$$E_{11}(k_1) = \frac{2}{\pi} \langle u^2 \rangle \int_0^{\infty} f(r_1) \cos(k_1 r_1) dr_1$$

- The Taylor micro and integral length scales are given by:

$$\lambda_f = \left[\frac{-2}{f''(0)} \right]^{\frac{1}{2}}$$

$$\Lambda_f = \frac{1}{2} \int_{-\infty}^{\infty} f(r) dr = \int_0^{\infty} f(r) dr$$

- Dissipation calculated from isotropic turbulence theory:

$$\varepsilon = \frac{30\nu \langle u^2 \rangle}{\lambda_f^2}$$

- Kolmogorov scale:

$$\eta = \left(\frac{\nu^3}{\varepsilon} \right)^{1/4}$$

- **Antisymmetric spatial autocorrelation function:**

$$f(\pm r) = \frac{\langle u(x)u(x \pm r) \rangle}{\langle u^2 \rangle}$$

- Fourier transform of $f(r)$ gives $E_{11}(k_1)$:

$$E_{11}(k_1) = \frac{\langle u^2 \rangle}{\pi} \int_{-\infty}^{\infty} f(r_1) \cos(k_1 r_1) dr_1$$

- The Taylor micro and integral length scales are given by:

$$\lambda_f = \frac{\left[-f'(0) - \left[\{f'(0)\}^2 - 2f''(0) \right]^{\frac{1}{2}} \right]}{f''(0)}$$

$$\Lambda_f = \frac{1}{2} \int_{-\infty}^{\infty} f(r) dr$$

- Dissipation calculated directly from its definition:

$$\varepsilon = \nu \left(\left(\frac{\partial u_i}{\partial x_j} \right)^2 + \frac{\partial u_i}{\partial x_j} \frac{\partial u_j}{\partial x_i} \right)$$

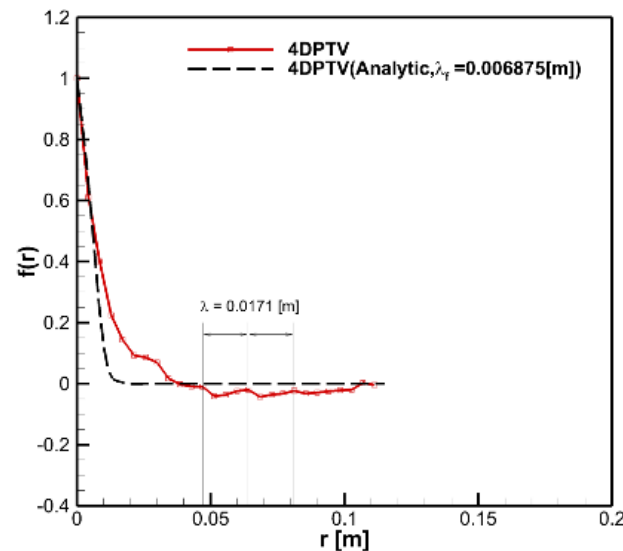
- Kolmogorov scale:

$$\eta = \left(\frac{\nu^3}{\varepsilon} \right)^{1/4}$$

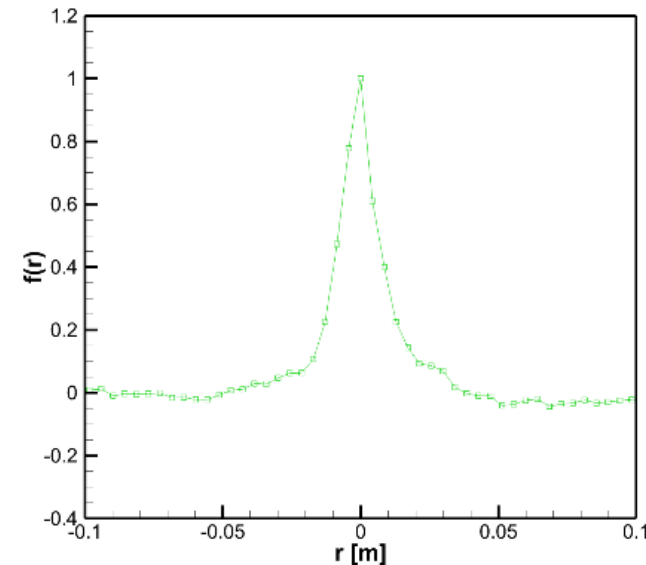
- Analytical spatial autocorrelation:

$$f(r) = e^{-\frac{r^2}{\lambda_f^2}}$$

- $f(r)$ shows Gaussian shape and good agreement analytical formula; $f(\pm r)$ shows asymmetric Gaussian shape. Asymmetry needs analysis and comparisons with Gaussian higher higher-order moments.
- The 4DPTV spatial resolution used for the current analysis is about 0.004277 m such that $l_{1\min} = 2dx = 0.009\text{m}$ and $l_{1\max} = 0.222\text{ m}$, the latter of which corresponds to the length of the measurement volume. The 4DPTV dr intervals and r_{\max} correspond to the previously mentioned dx and $l_{1\max}$ values, respectively.
- Both distributions show periodic behavior with wavelength $\lambda = 0.0171\text{ m}$, which is attributed the Kelvin-Helmholtz instability of the shear layer that wraps around the spiral vortex.

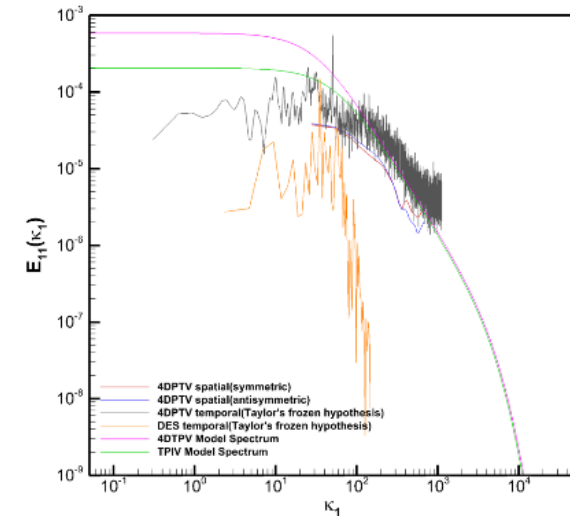


Symmetric spatial Longitudinal
Correlation Coefficient.

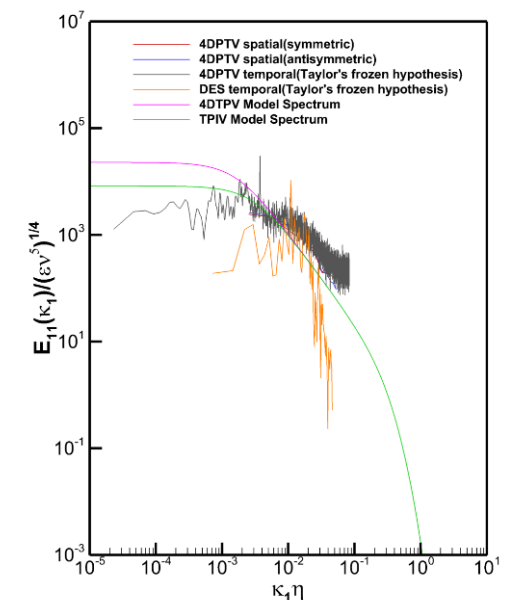
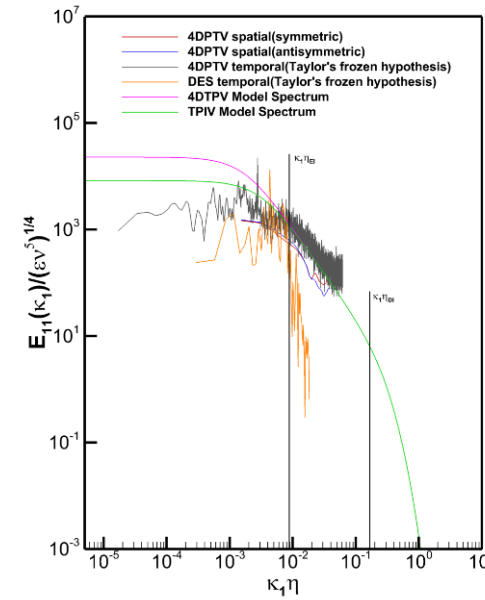


Anti-symmetric spatial Longitudinal
Correlation Coefficient.

- $E_{11}(\kappa_1)$ shows that the 4DPTV resolves a larger portion of the inertial subrange with the Kolmogorov $-5/3$ slope, whereas the DES is only able to partially resolve the inertial sub range and then dissipates rapidly. The rapid dissipation is likely because of the lack of filter/grid resolution as often exhibited in LES.
- The spatial spectrum ranges are limited to the inertial sub range, showing less energy than the 4DPTV temporal spectrum using the Taylor hypothesis, and exhibit kinks in the region of their largest wave numbers, which is attributed to the 4DPTV minimum spatial resolution.
- The 4DPTV and TPIV model spectrums overlap in the inertial and dissipation ranges, whereas the 4DPTV has larger magnitudes than the TPIV in the energy containing ranges as expected due to its larger u' value.
- It should be noted that the model spectrums for the 4DPTV and TPIV overpredict the energy magnitude (i.e., $\langle u^2 \rangle$) within the energy-containing range as isotropic turbulence assumptions scale the model spectrum by u'^2 .
- The 4DPTV can resolve a large portion of the inertial subrange including the correct Kolmogorov constant. The linear behavior observed for large wave numbers ($\kappa_1 \eta > 0.3$) indicates exponential decay.

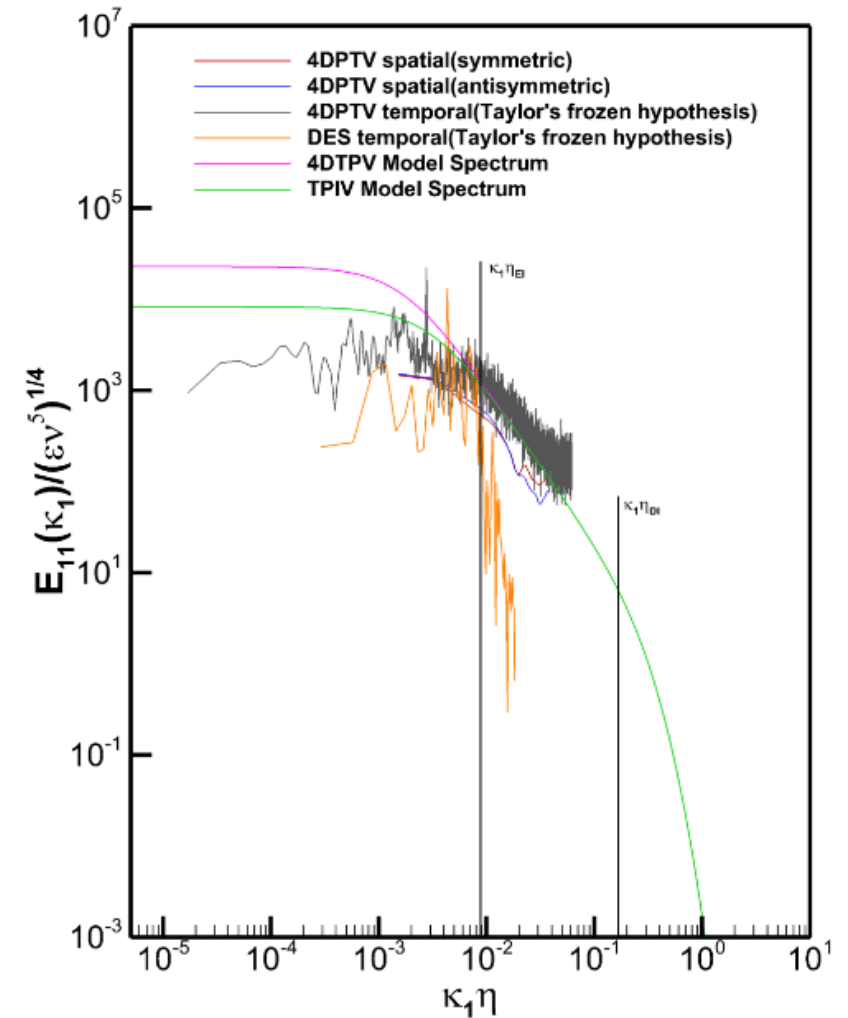


1D longitudinal velocity spectra.



1D longitudinal velocity spectra shown for Kolmogorov scaling using (left) macro-scale values and (right) micro-scale values

- The κ_1 values corresponding to the beginning of the inertial subrange ($\kappa_{1,EI}$), and dissipation range ($\kappa_{1,DI}$), are labeled. The $k_{1,EI}$ values corresponds to the range (i.e., $0 < k_1 < \kappa_{1,EI}$) containing 80% of the integral value of the model E_{11} spectrum, u'^2 .
- The start of the dissipation subrange is established using the peak of dissipation spectrum as discussed in Pope (2000) and Bernard (2019).
- Pope (2000) Figure 6.16 shows that for isotropic decaying turbulence (for $R_\lambda = 600$) the peak of the dissipation spectrum is around $\frac{1}{\eta} \sim 24$ and that the bulk of the dissipation occurs for $60 > 1/\eta > 8$. Similarly, experimental studies mentioned by Bernard (2019) show that the peak of the dissipation spectrum is at $\frac{1}{\eta} \sim 40 - 60$.
- The other way to establish the start of dissipation subrange is using Taylor's micro-scale. Using the definition of η and $\varepsilon \sim \nu u_{rms}^2 / \lambda^2$ one can show that $\frac{\lambda}{\eta} = \sqrt{R_\lambda}$, suggesting that the dissipation subrange is wider for larger R_λ . This is consistent with isotropic decaying turbulence experiments by Kang et al. (2003), wherein λ/η increased from 49 to 53 when R_λ increased from 626 to 716.
- The averaged R_λ estimate in this study is 570, thus based on $\frac{\lambda}{\eta}$ range above, a reasonable estimate should be $l_{DI} \sim 50\eta$. Therefore, $l_{DI} \sim 60\eta$ used in the study represents an upper limit of the demarcation between the inertial and dissipation range.



1D longitudinal velocity spectra shown for Kolmogorov scaling using macro-scale values.

Spectral Analysis and Small Scales: Micro-scale parameters

- The benchmark λ_f is 2.5 mm, which is about half the size of the 4DPTV spatial resolution used for the present analysis. The lack of spatial resolution causes the 4DPTV to severely overpredict the value of λ_f (+150% on average) compared to the benchmark. Therefore, the current 4DPTV spatial resolution is insufficient as sub mm spatial resolution is required to resolve the Taylor micro-scale.
- The discrepancy in λ_f affects the estimates of R_λ , ε , and η , causing an overprediction of R_λ and η and an underprediction of the dissipation ε .
- Both the micro-scale benchmark estimates for the 4DPTV and TPIV are of similar orders of magnitude; however, the TPIV estimates for the Taylor micro and macro-scales and turbulent Reynolds number are smaller and its Kolmogorov length scale is larger. As observed for the 4DPTV, the λ_f benchmark is on the order of their spatial resolutions (1mm TPIV, 4mm 4DPTV). This reiterates the need for sub mm spatial resolution to resolve the Taylor micro-scale.

Parameter	4DPTV Macro-Scale BM Estimates	Temporal (T) 4DPTV	T % 4DPTV BM	Spatial Symmetric (SS)	SS % 4DPTV BM	Spatial Antisymmetric and Anisotropic (SAA)	SAA % 4DPTV BM
λ_f [m]	2.50E-03	4.59E-03	83.60%	6.87E-03	174.80%	7.20E-03	188.00%
Λ_f [m] = $L_{11}=l_o$	2.50E-02	7.59E-03	-69.64%	8.69E-03	-65.24%	9.63E-03	-61.48%
R_λ	3.27E+02	4.92E+02	50.46%	7.35E+02	124.77%	7.71E+02	135.78%
ε [m ² /s ³]	1.81E-01	5.38E-02	-70.28%	2.40E-02	-86.74%	2.19E-02	-87.90%
η [m]	5.50E-05	7.44E-05	35.27%	9.10E-05	65.45%	9.32E-05	69.45%

4DTPV Microscale Vortex Core Parameters.

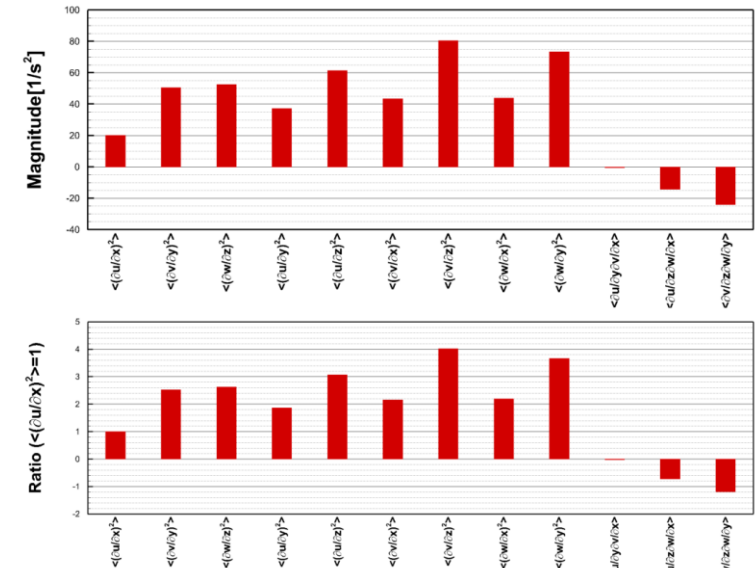
Parameter	4DPTV Macro-Scale BM Estimates	TPIV Macro-Scale BM Estimates	TPIV Macro-Scale % 4DPTV Macro-Scale	DES Temporal	DES % 4DPTV BM	DES % TPIV BM	DES % Temporal 4DPTV
λ_f [m]	2.50E-03	2.11E-03	-15.60%	3.48E-02	1292.00%	1549.29%	658.17%
Λ_f [m] = $L_{11}=l_o$	2.50E-02	1.40E-02	-44.00%	4.60E-02	84.00%	228.57%	506.06%
R_λ	3.27E+02	2.19E+02	-33.03%	1.61E+03	392.35%	635.16%	227.24%
ε [m ² /s ³]	1.81E-01	1.60E-01	-11.60%	1.76E-04	-99.90%	-99.89%	-99.67%
η [m]	5.50E-05	5.70E-05	3.64%	3.11E-04	465.45%	445.61%	318.01%

TPIV, DES, and 4DTPV Microscale Vortex Core Parameters.

Spectral Analysis and Small Scales: Anisotropy of the dissipation

- Isotropic relationships for dissipation tensor components prior to contraction:

- $\langle \left(\frac{\partial u}{\partial x}\right)^2 \rangle = \langle \left(\frac{\partial v}{\partial y}\right)^2 \rangle = \langle \left(\frac{\partial w}{\partial z}\right)^2 \rangle$
- $\langle \left(\frac{\partial u}{\partial y}\right)^2 \rangle = \langle \left(\frac{\partial u}{\partial z}\right)^2 \rangle = \langle \left(\frac{\partial v}{\partial x}\right)^2 \rangle = \langle \left(\frac{\partial v}{\partial z}\right)^2 \rangle = \langle \left(\frac{\partial w}{\partial x}\right)^2 \rangle = \langle \left(\frac{\partial w}{\partial y}\right)^2 \rangle = 2 \langle \left(\frac{\partial u}{\partial x}\right)^2 \rangle$
- $\left\langle \frac{\partial u}{\partial y} \cdot \frac{\partial v}{\partial x} \right\rangle = \left\langle \frac{\partial u}{\partial z} \cdot \frac{\partial w}{\partial x} \right\rangle = \left\langle \frac{\partial v}{\partial z} \cdot \frac{\partial w}{\partial y} \right\rangle = -\frac{1}{2} \langle \left(\frac{\partial u}{\partial x}\right)^2 \rangle$



Dimensional and normalized (by $\langle (\partial u/\partial x)^2 \rangle$) dissipation components.

- Dissipation tensor components prior to contraction show large anisotropy:

- $\langle \left(\frac{\partial v}{\partial y}\right)^2 \rangle \approx \langle \left(\frac{\partial w}{\partial z}\right)^2 \rangle$ and nearly 3 x $\langle \left(\frac{\partial u}{\partial x}\right)^2 \rangle$.
- $\langle \left(\frac{\partial u}{\partial y}\right)^2 \rangle \approx \langle \left(\frac{\partial v}{\partial x}\right)^2 \rangle \approx \langle \left(\frac{\partial w}{\partial x}\right)^2 \rangle \approx 2 \langle \left(\frac{\partial u}{\partial x}\right)^2 \rangle$, i.e., show isotropic behavior.
- Whereas $\langle \left(\frac{\partial u}{\partial z}\right)^2 \rangle$, $\langle \left(\frac{\partial v}{\partial z}\right)^2 \rangle$, and $\langle \left(\frac{\partial w}{\partial y}\right)^2 \rangle$ are 3-4 times $\langle \left(\frac{\partial u}{\partial x}\right)^2 \rangle$.
- $\left\langle \frac{\partial u}{\partial y} \cdot \frac{\partial v}{\partial x} \right\rangle \approx 0$ and $\left\langle \frac{\partial u}{\partial z} \cdot \frac{\partial w}{\partial x} \right\rangle \approx \left\langle \frac{\partial v}{\partial z} \cdot \frac{\partial w}{\partial y} \right\rangle \approx -\left\langle \left(\frac{\partial u}{\partial x}\right)^2 \right\rangle$ vs. $= -\frac{1}{2} \langle \left(\frac{\partial u}{\partial x}\right)^2 \rangle$

Components	Magnitude [1/s ²]	Ratio (Normalized by $\langle (\partial u/\partial x)^2 \rangle$)
$\langle (\partial u/\partial x)^2 \rangle$	2.003E+01	1.00
$\langle (\partial v/\partial y)^2 \rangle$	5.050E+01	2.52
$\langle (\partial w/\partial z)^2 \rangle$	5.260E+01	2.63
$\langle (\partial u/\partial y)^2 \rangle$	3.725E+01	1.86
$\langle (\partial u/\partial z)^2 \rangle$	6.144E+01	3.07
$\langle (\partial v/\partial x)^2 \rangle$	4.335E+01	2.16
$\langle (\partial v/\partial z)^2 \rangle$	8.046E+01	4.02
$\langle (\partial w/\partial x)^2 \rangle$	4.388E+01	2.19
$\langle (\partial w/\partial y)^2 \rangle$	7.346E+01	3.67

Partial Derivative Components for 4DPTV.

- The Reynolds stresses can be decomposed into their isotropic and anisotropic components:

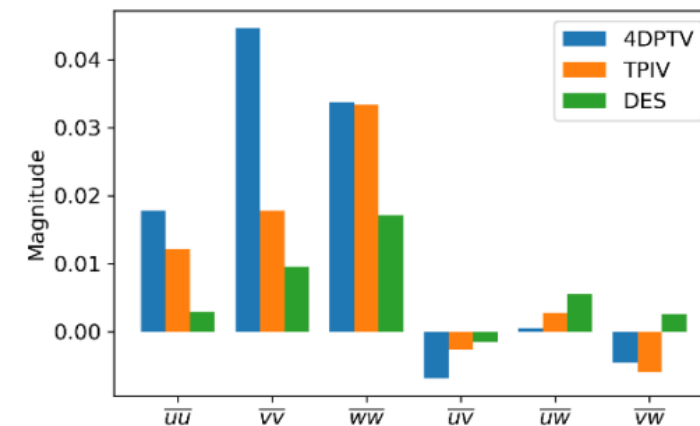
$\mathcal{R}_{ij}(\underline{x}, t) = a_{ij} + \frac{2}{3}k\delta_{ij}$, where a_{ij} is the anisotropic Reynolds stress tensor and k is the turbulent kinetic energy. a_{ij} can be normalized using a factor equal to $2k$ to obtain the normalized anisotropic Reynolds stress b_{ij} :

$$\mathcal{R}_{ij}(\underline{x}, t) = \begin{pmatrix} \overline{uu} & \overline{uv} & \overline{uw} \\ \overline{vu} & \overline{vv} & \overline{vw} \\ \overline{wu} & \overline{wv} & \overline{ww} \end{pmatrix} \quad b_{ij} = \begin{pmatrix} \frac{\overline{uu}}{2k} - \frac{1}{3} & \frac{\overline{uv}}{2k} & \frac{\overline{uw}}{2k} \\ \frac{\overline{vu}}{2k} & \frac{\overline{vv}}{2k} - \frac{1}{3} & \frac{\overline{vw}}{2k} \\ \frac{\overline{wu}}{2k} & \frac{\overline{wv}}{2k} & \frac{\overline{ww}}{2k} - \frac{1}{3} \end{pmatrix} \quad \frac{2}{3}k\delta_{ij} = \begin{pmatrix} \frac{2}{3}k & 0 & 0 \\ 0 & \frac{2}{3}k & 0 \\ 0 & 0 & \frac{2}{3}k \end{pmatrix}$$

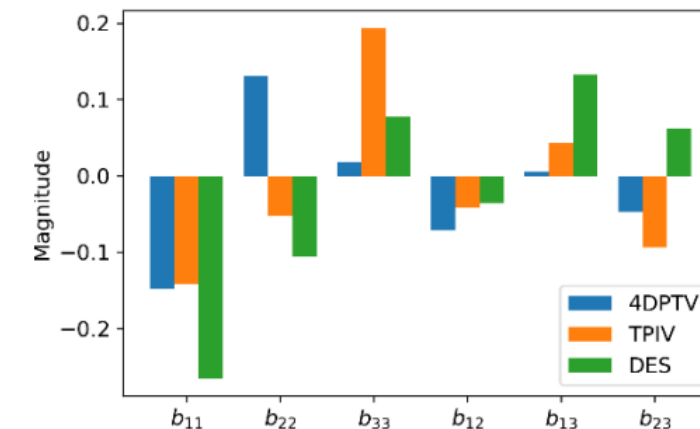
- The conditions for the positive semi-definiteness of the Reynolds stress tensor can be expressed as constraints on the values of b_{ij} (Banerjee et al., 2007):

$$-\frac{1}{3} \leq b_{11}, b_{22}, b_{33} \leq \frac{2}{3} \quad \text{and} \quad -\frac{1}{2} \leq b_{ij} \leq \frac{1}{2}, i \neq j$$

- The 4DPTV exhibits larger values for all three normal Reynolds stresses compared to TPIV and DES. On the other hand, the DES displays the smallest values for \overline{uu} , \overline{vv} and \overline{ww} . Consequently, the turbulent kinetic energy of the 4DPTV is approximately three times larger than that of the DES.
- The trend for \overline{uv} and \overline{uw} is similar among all three methods, with differences in magnitude. DES shows the opposite sign compared to 4DPTV and TPIV for \overline{vw} .
- The normal components of b_{ij} show that DES, 4DPTV, and TPIV have the largest values for b_{11} , b_{22} , b_{33} , respectively. It is important to notice that b_{22} for TPIV and DES shows the opposite sign compared to the 4DPTV.



Comparison of Reynolds stress components: 4DPTV, TPIV, and DES.



Comparison of anisotropic Reynolds stress components: 4DPTV, TPIV, and DES.

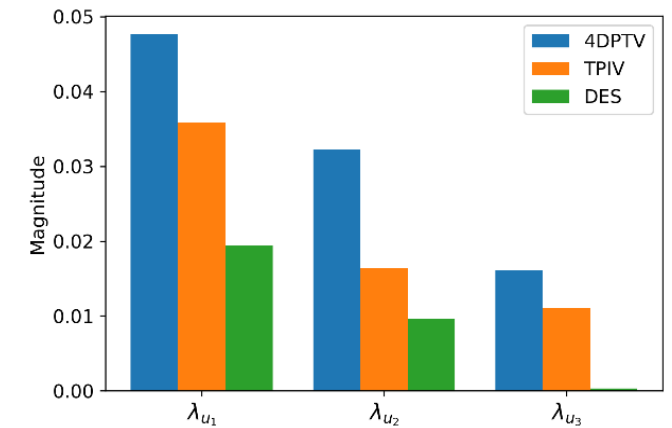
- The eigenvalue problem for R_{ij} and b_{ij} provides their characteristic equations (cubic polynomials) with three principal invariants which are independent of reference frame and functions of their respective components, i.e., $\overline{u_i u_j}$ and $\frac{a_{ij}}{2k}$, respectively.

$$\lambda^3 - I_b \lambda^2 + II_b \lambda - III_b = 0$$

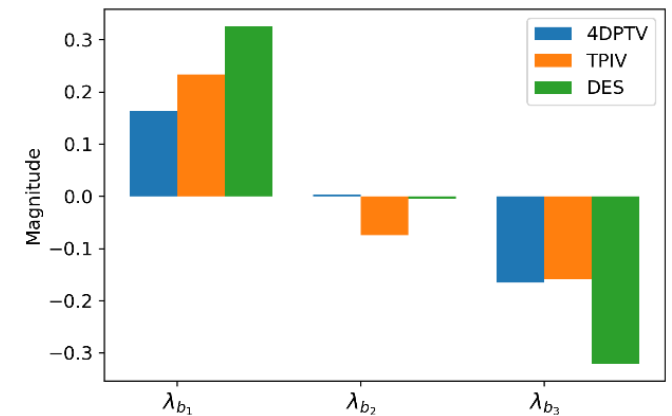
- Since b_{ij} has zero trace, only two of its invariants/eigenvalues are independent. Additionally, the eigenvalues of R_{ij} , here referred to as λ_{u_i} , are related to the eigenvalues of b_{ij} as follows:

$$\lambda_{b_i} = -\frac{1}{3} + \frac{\lambda_{u_i}}{\lambda_{u_1} + \lambda_{u_2} + \lambda_{u_3}} \quad (1)$$

- The eigenvalues of the Reynolds stress are ordered in descending order, i.e., λ_{u_1} is the largest. The 4DPTV exhibits the largest eigenvalues for R_{ij} , followed by TPIV, and DES.
- Note that while λ_{u_1} is the largest eigenvalue for the Reynolds stress, the eigenvalues of b_{ij} are not ordered in descending order but given by Equation (1). Largest values for λ_{b_2} and λ_{b_3} are for DES, whereas TPIV exhibits maximum λ_{b_1} . The sign of λ_{b_2} is negative for TPIV and DES and positive for 4DPTV. This fact has important consequences for the location of the turbulence in the Lumley triangle.



Comparison of Reynolds stress eigenvalues: 4DPTV, TPIV, and DES.



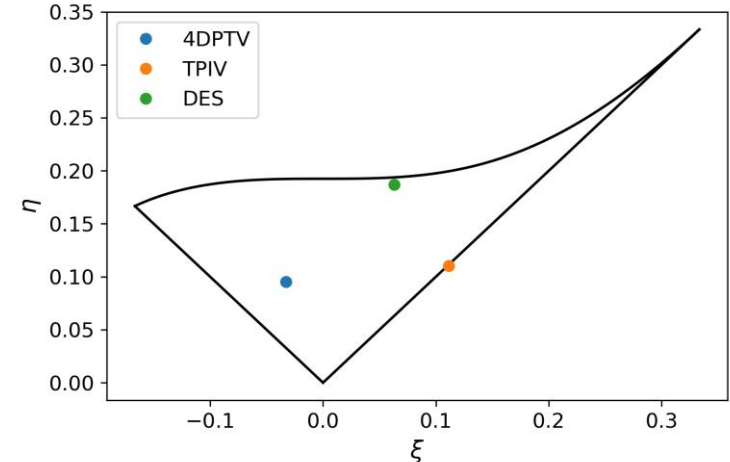
Comparison of anisotropic Reynolds stress eigenvalues: 4DPTV, TPIV, and DES.

Turbulence Anisotropy: Lumley triangle and Anisotropic Invariant Map

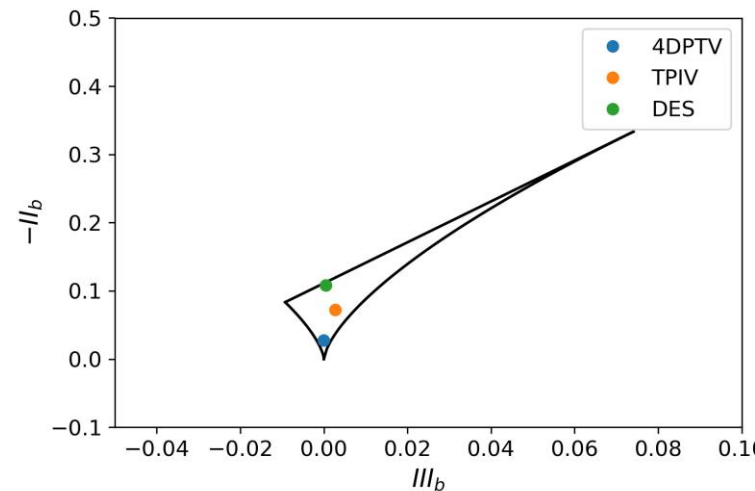
- The states of realizable turbulence can be shown in terms of the invariants (Π_b and III_b , Anisotropic Invariant Map (AIM)) or eigenvalues (η and ξ , Lumley triangle) of b_{ij} :

$$\begin{aligned} II_b &= -3\eta^2 = -(\lambda_{b_1}^2 + \lambda_{b_1}\lambda_{b_2} + \lambda_{b_2}^2) \\ III_b &= 2\xi^3 = -\lambda_{b_1}\lambda_{b_2}(\lambda_{b_1} + \lambda_{b_2}) \end{aligned}$$

- Based on the eigenvalues of b_{ij} , the invariants of the turbulence are evaluated and represented on the Lumley triangle and Anisotropic Invariant Map (AIM).
- 4DPTV shows a negative value for ξ (III_b), whereas this quantity is positive for both DES and TPIV. The magnitude of η ($-II_b$) is largest for DES, and almost two times larger than TPIV and 4DPTV.
- DES predicts a turbulence state very close to the two-component limit, whereas 4DPTV is closer to an axisymmetric contraction.
- For TPIV and DES, the change of sign in λ_{b_2} determines a positive value for ξ (III_b). Consequently, for TPIV the turbulence state is almost on the right border of the Lumley triangle, corresponding to an axisymmetric expansion.
- The components of R_{ij} and b_{ij} are related to their eigenvalues by a non-linear system and it is not trivial to understand the contribution of each element of the Reynolds stress tensor in the anisotropy. However, the magnitudes of the normal stresses are much larger compared to the shear stress terms, which could indicate that they play a dominant role in determining the eigenvalues and eigenvectors of the Reynolds stress tensor.



Lumley triangle with 4DPTV, TPIV, and DES realizations.

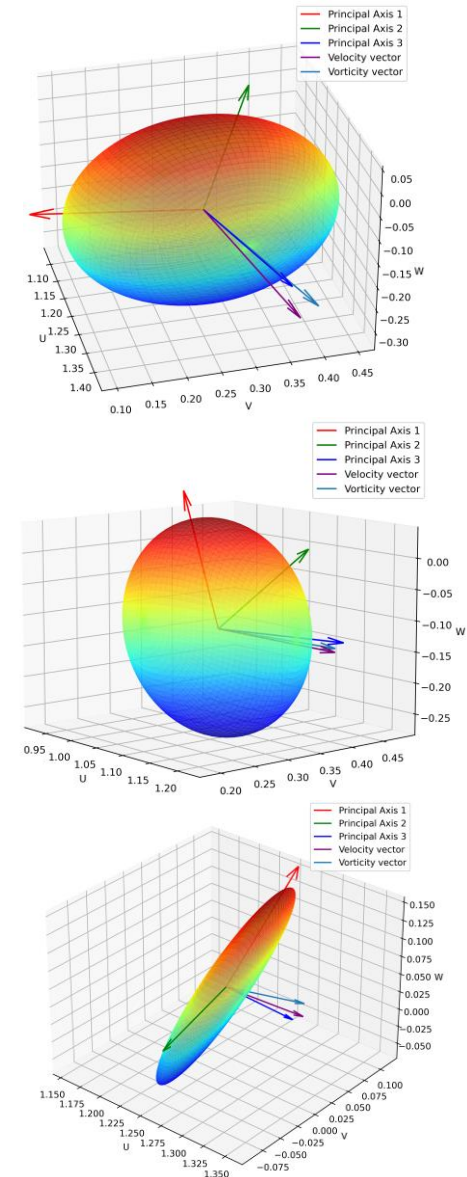


Anisotropic invariant map with 4DPTV, TPIV, and DES realizations.

- The Reynolds stress ellipsoid is defined by the expected value equation $E(\mathbf{U}, \alpha) \leq 1$ for given constant $\alpha \geq 0$ (assumed equal to 1) with solution given by:

$$\left(\frac{U_1 - \bar{U}_1}{\sqrt{\lambda_{u_1}}}\right)^2 + \left(\frac{U_2 - \bar{U}_2}{\sqrt{\lambda_{u_2}}}\right)^2 + \left(\frac{U_3 - \bar{U}_3}{\sqrt{\lambda_{u_3}}}\right)^2 \leq 1$$

- This represents an ellipsoid centered in $(\bar{U}_1, \bar{U}_2, \bar{U}_3)$ with the half-lengths of the principal axes being $\sqrt{\lambda_{u_i}}$. Therefore, the ellipsoid represents the volume in velocity space of the realizable fluctuations of the turbulence at the vortex core.
- For 4DPTV, $\sqrt{\lambda_{u_1}} \sim 1.2\sqrt{\lambda_{u_2}} \sim 1.7\sqrt{\lambda_{u_3}}$ implies that the semi-axes in the x_{R_1} and x_{R_2} directions are very close in magnitude, whereas the third direction is almost half in length. This confirms that the shape of the ellipsoid is close to an oblate spheroid, where $\sqrt{\lambda_{u_1}} = \sqrt{\lambda_{u_2}} > \sqrt{\lambda_{u_3}}$.
- For TPIV, $\sqrt{\lambda_{u_1}} \sim 1.5\sqrt{\lambda_{u_2}} \sim 1.8\sqrt{\lambda_{u_3}}$ such that the semi-axis in the x_{R_1} direction is larger than the other two directions. In this case, the ellipsoid resembles a prolate spheroid, where $\sqrt{\lambda_{u_1}} > \sqrt{\lambda_{u_2}} = \sqrt{\lambda_{u_3}}$.
- DES exhibits a more flattened shape, with $\sqrt{\lambda_{u_1}} \sim 1.4\sqrt{\lambda_{u_2}} \sim 7.4\sqrt{\lambda_{u_3}}$ and the ellipsoid collapses into an almost 2D elliptical disc, where $\sqrt{\lambda_{u_1}} > \sqrt{\lambda_{u_2}}$ and $\sqrt{\lambda_{u_3}} = 0$. This characteristic shape is typical of 2D turbulence.



Reynolds stress ellipsoids; (top) 4DPTV, (mid) TPIV, and (bottom) DES. The velocity and vorticity vectors are scaled by their magnitude multiplied by a constant.

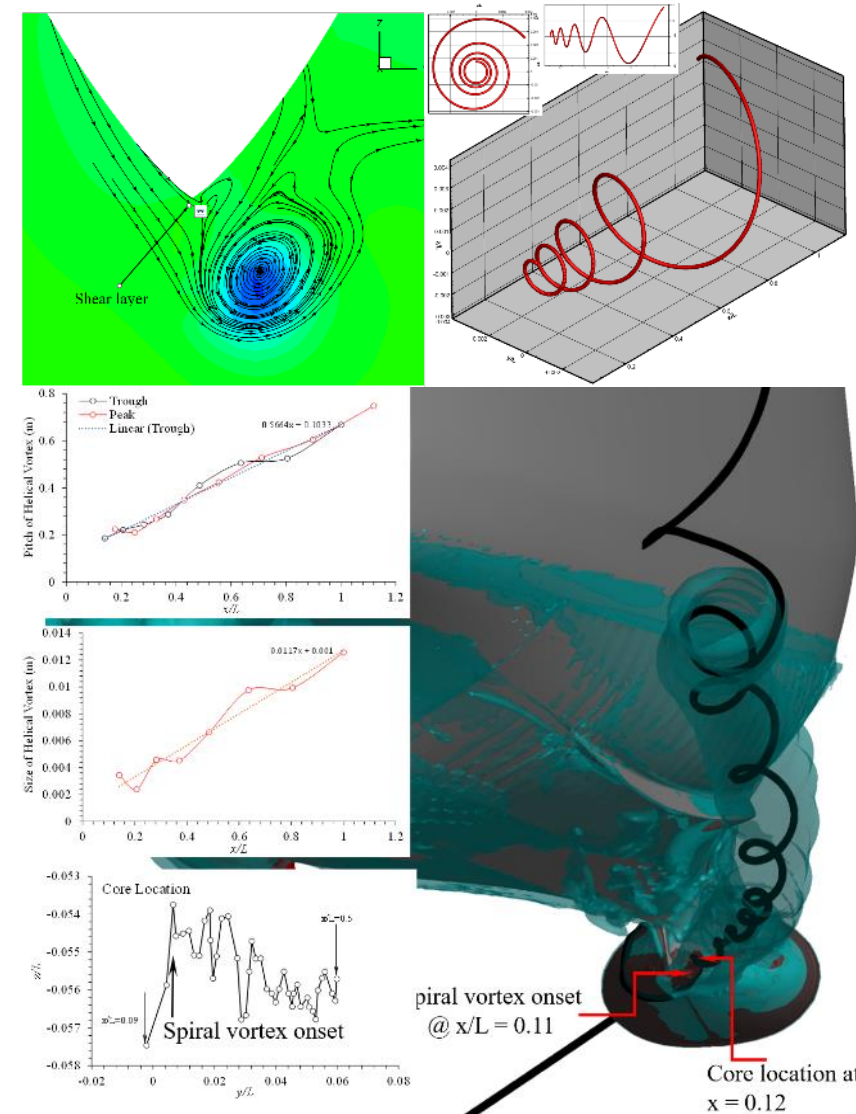
- The principal axis associated with the largest eigenvalue indicates the direction where the velocity fluctuations are most pronounced. For the 4DPTV, this almost coincides with the second component of the velocity (V), whereas both the TPIV and DES exhibit a predominant alignment with the third component (W). This difference is attributed to the fact that for the 4DPTV the largest normal Reynolds stress is $\overline{v'v'}$, whereas for the TPIV and DES it is $\overline{w'w'}$.
- For 4DPTV and TPIV, the principal axis associated with the largest eigenvalue is nearly perpendicular to the direction of the mean velocity vector. This indicates that the maximum fluctuations of the velocity vector occur in a plane that is perpendicular to the mean velocity direction. In the case of DES, the angle is around 71 deg.
- More generally, the plane generated by $x_{\mathcal{R}_1}$ and $x_{\mathcal{R}_2}$ is almost perpendicular to the velocity vector, such that the angle between $x_{\mathcal{R}_3}$ and \overline{U} is less than 10 deg for 4DPTV and TPIV, and 20 deg for DES. Therefore, the turbulence, which is strongest at the vortex core, is diffused almost perpendicular to its axis.
- The direction of the principal axes depends on the Reynolds stress tensor eigenvalues and, more generally, on the Reynolds stress tensor components.

	Semi-axes of the RS ellipsoid			Angle between RS ellipsoid principal axes and \overline{U} [deg]			Angle between RS ellipsoid principal axes and $\overline{\Omega}$ [deg]		
	$\sqrt{\lambda_{u_1}}$	$\sqrt{\lambda_{u_2}}$	$\sqrt{\lambda_{u_3}}$	$x_{\mathcal{R}_1} \cdot \overline{U}$	$x_{\mathcal{R}_2} \cdot \overline{U}$	$x_{\mathcal{R}_3} \cdot \overline{U}$	$x_{\mathcal{R}_1} \cdot \overline{\Omega}$	$x_{\mathcal{R}_2} \cdot \overline{\Omega}$	$x_{\mathcal{R}_3} \cdot \overline{\Omega}$
4DPTV	0.219	0.180	0.127	91.14	98.07	8.13	99.63	96.37	11.57
TPIV	0.189	0.128	0.105	93.81	95.60	6.02	94.28	90.49	4.33
DES	0.139	0.098	0.019	70.80	73.13	26.01	73.99	87.10	16.28

Characteristics of the Reynolds Stress Ellipsoid and its Orientation vs. Mean Velocity and Mean Vorticity Vectors for 4DPTV, TPIV, and DES.

Vortex Breakdown and Interaction (1)

- Xing et al. (2012) identified spiral vortex breakdown followed by helical mode instability in their DES for KVLCC2 at $\beta = 30$ deg and its analogy with delta wing flows; however, experimental validation is still not available for KVLCC2.
- Bhushan et al. (2019, 2021) DES for 5415 at $\beta = 20$ deg showed similar vortex breakdown characteristic as KVLCC2 and this time with TPIV validation for St and St_{Ds} .
- It should be noted that ship flow geometries and separation types are mostly different than delta wings, i.e., smooth surfaces with crossflow and bubble type separations vs. sharp edges with sharp edge separations for delta wings, except for bilge keels and other similar appendages with sharp edges for ships.
- The top left figure shows planar streamlines at $x/L = 0.12$. The flow spirals inwards towards the vortex core, indicating the presence of a spiral vortex breakdown. The shear layer due to the crossflow around the keel wraps around the vortex core.
- The bottom right figure shows the upstream streamline that merges into and emerges from the vortex core at $x/L = 0.12$. The vortex core is identified by the high $Q = 10000$ value iso surface (red). The transparent iso surface in blue is for $Q = 100$, which shows the primary vortex structure.



Planar streamlines at $x/L = 0.12$ showing the spiral vortex (upper left); model for the helical path of the vortex core from $x/L = 0.11$ to $x/L = 1$ (upper right); and helical instability emerging from the spiral vortex breakdown at $x/L = 0.11$, including inserted plots showing the pitch of the helix, size of the helix, and helix core locations (lower).

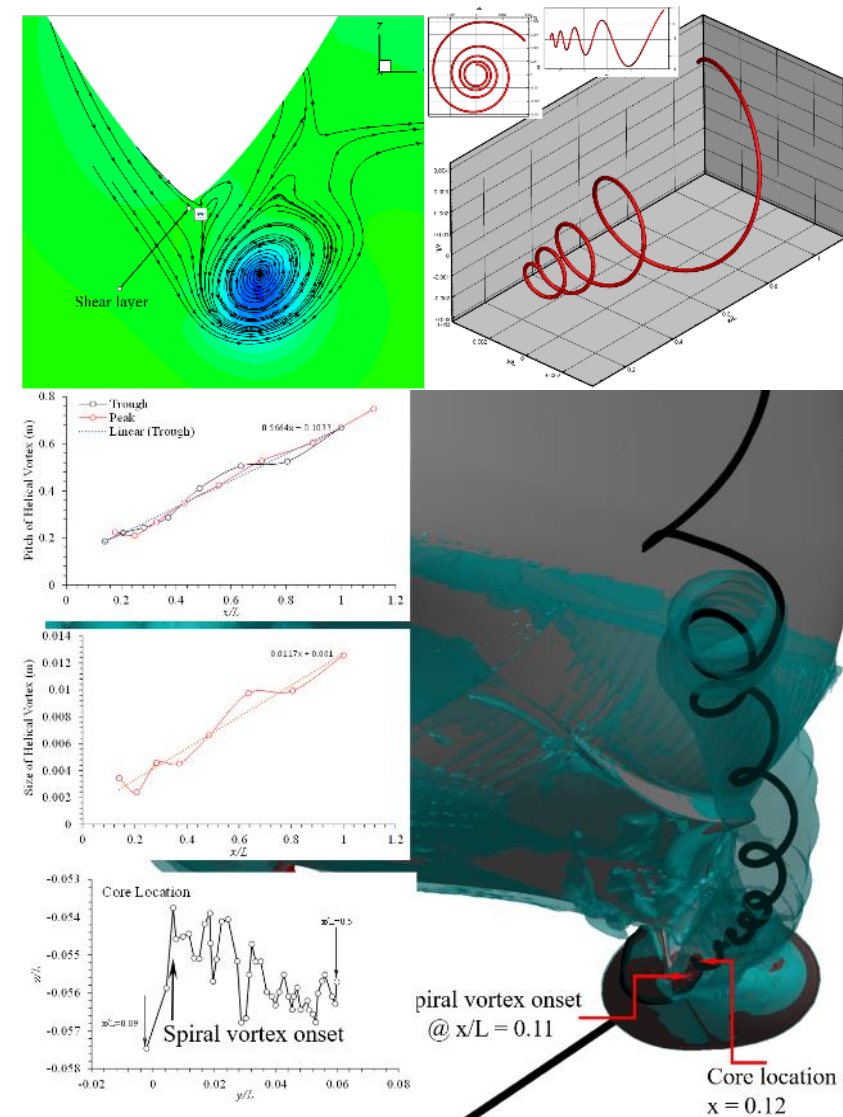
Vortex Breakdown and Interaction (2)

- The left middle upper inset plot shows the pitch of the helical vortex. The pitch increases linearly with progression with values of around 0.2 m at onset to 0.75 m aft of the stern.
- The left middle lower inset plot shows the estimated size of the helical vortex, which also increases linearly with distance from onset.
- The left bottom inset plot shows the vortex core location that was manually extracted from the peak Q values at slices of $x/L = 0.09$ to 0.5 at every 0.01L. The vortex core shows an upwards drift between $x/L = 0.09$ to 0.11, and then shows unsteady helical motion.
- The top right figure shows a model for the helical path of the vortex core from $x/L = 0.11$ to $x/L = 1$. The inset plots show the view of the helical path in the y-z and x-z planes. The helical path is obtained using the equations:

$$y/L = A(x/L) \sin(\omega(x/L) \times x/L)$$

$$z/L = A(x/L) \cos(\omega(x/L) \times x/L)$$

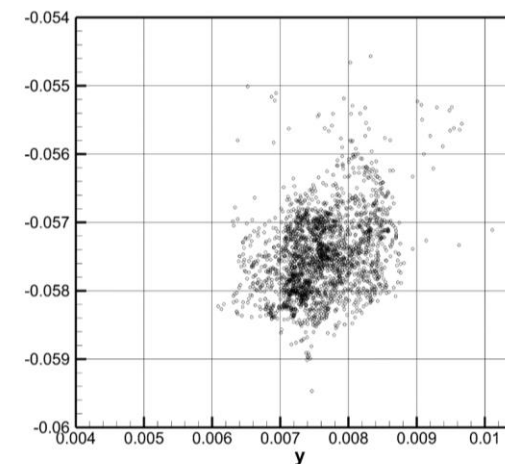
- The frequency $\omega(x/L)$ is estimated from the pitch of the helical vortex, which gives $\omega(x/L) = 2\pi L / (0.1 + 0.5664x)$. The amplitude is estimated from the size of the helical vortex, which gives $A(x/L) = (0.001 + 0.0117x) / L$.



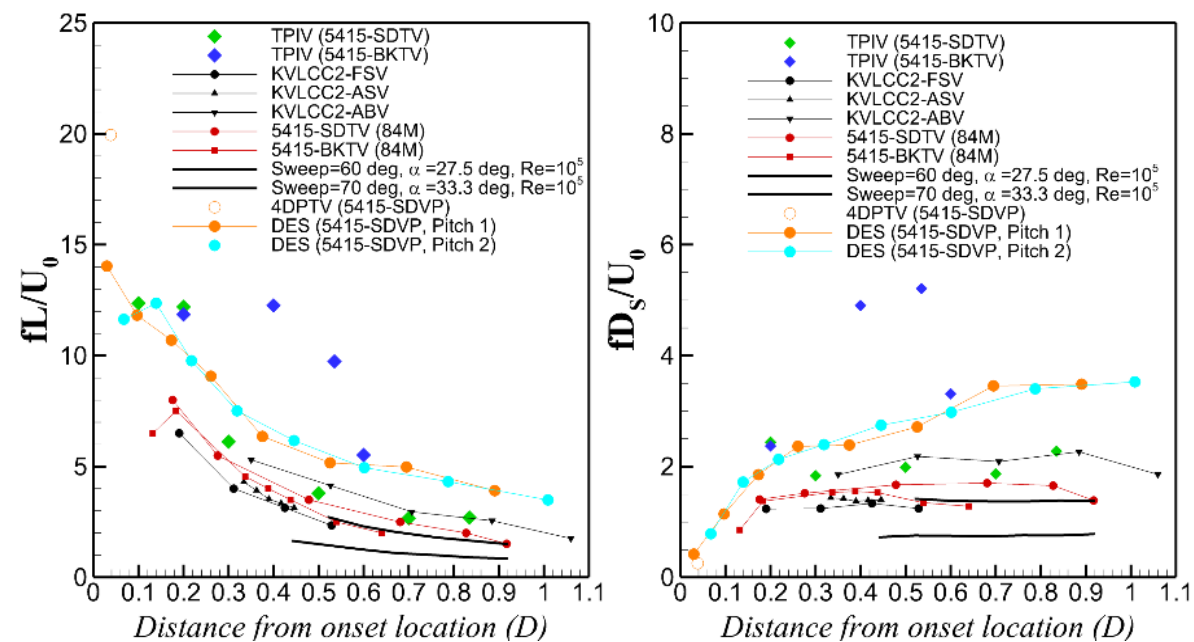
Planar streamlines at $x/L = 0.12$ showing the spiral vortex (upper left); model for the helical path of the vortex core from $x/L = 0.11$ to $x/L = 1$ (upper right); and helical instability emerging from the spiral vortex breakdown at $x/L = 0.11$, including inserted plots showing the pitch of the helix, size of the helix, and helix core locations (lower).

Vortex Breakdown and Interaction (3)

- The streamlines in the SDVP vortex undergo transition from straight to helical with the spiral vortex breakdown estimated to occur at about $x/L = 0.11$.
- The wave-length of the $u(x, t)$ spatial waves and pitch of the helix vortex core at $x/L = 0.12$ closely agree. The linear growth for the helix pitch indicates the same frequency scaling as shown previously for KVLCC2 and 5415. This can be seen in the bottom figures representing the variation of St and St_{DS} vs. distance from onset.
- The top figure shows the instantaneous trajectory in the (y, z) plane at $x/L = 0.12$. The FFT of the SDVP at $x/L = 0.12$ core coordinates and displacement velocity were compared with the FFT of $u(x, t)$. All three variables show similar behavior.
- The turbulent axial velocity and vortex core displacement and velocity all show the footprint of the spiral vortex breakdown/helical mode instability.



Instantaneous SDVP vortex core (y, z) trajectory at $x/L=0.12$.

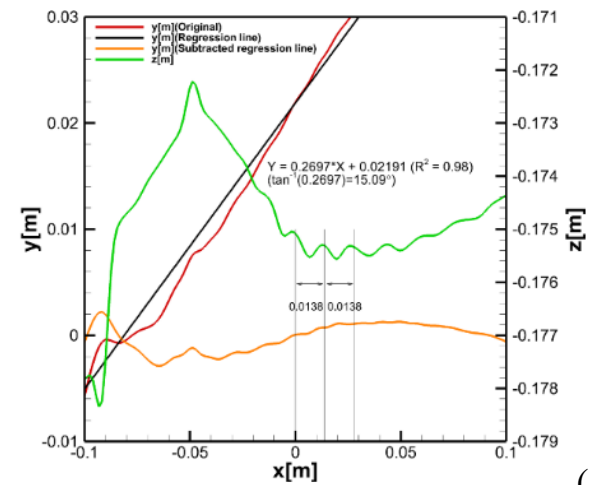


Variation of St and St_{DS} vs. distance from onset.

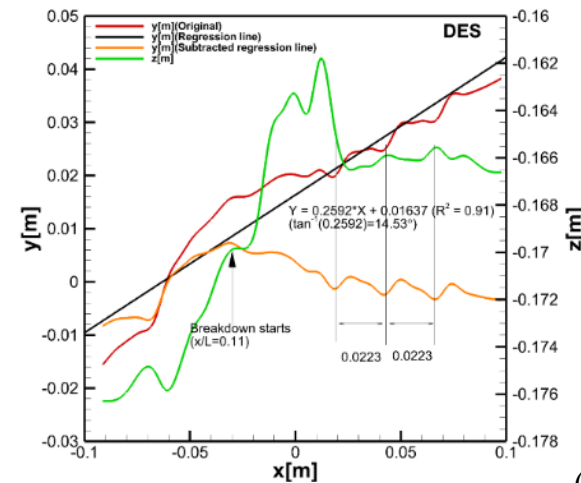
[SDVP-SDVS vortex breakdown and interaction.](#)

Vortex Breakdown and Interaction (4)

- The SDVP y coordinate trajectory is in line with the drift angle $\beta=10$ deg with somewhat larger values near its onset.
- The streamwise vortex core (y, z) trajectories show low frequency oscillations that correspond to the spiral vortex breakdown/helical mode instability and high frequency oscillations that correspond to those shown in the spatial autocorrelation
- Sanada et al. (2023) shows what appear to be shear layer vortices covering the surface of both the SDVP and SDVS vortices with wave lengths like those shown in the streamwise vortex core (y, z) trajectories.
- It is hypothesized that the high frequency oscillations of the streamwise vortex core (y, z) trajectories are due to the shear layer that wraps around the spiral vortices and its associated Kelvin-Helmholtz instability.
- However, it should be recognized that the resolution of the shear layer vortices and the Kelvin-Helmholtz instability is at the limit of the current 4DPTV resolution and as is also the case with resolving the Taylor micro scale increased resolution is required.
- Based on this, the SDVP wandering is due both to the spiral vortex breakdown/helical mode instability and the shear layer vortices.



(a)



(b)

4DPTV streamwise vortex core (y, z) trajectory coordinates and FFT (a); and DES streamwise vortex core (y, z) trajectory coordinates and global view of the SDVP vortex (b).

Conclusions and Future Research (1)

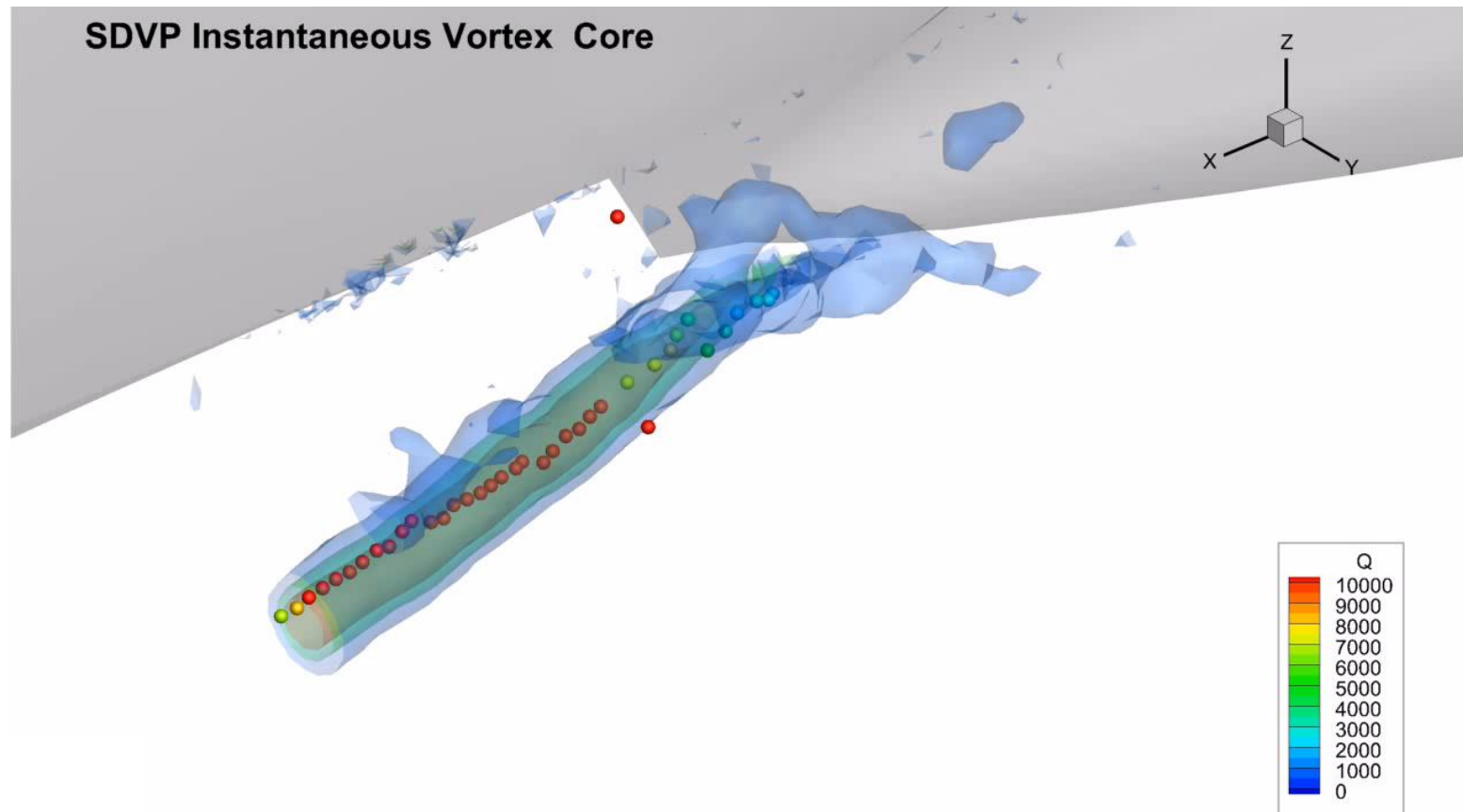
- Additional analysis of the 4DPTV static drift $\beta = 10$ deg results for the 5415 sonar dome vortices is made to realize its full potential for the assessment of the turbulence structure and vortex breakdown and interactions and for providing data for scale resolved CFD validation.
- The 4DPTV has increased capability compared to the previous TPIV in terms of measurement volume size and sampling rate, whereas it has less spatial resolution. The assessment includes comparisons with both the previous TPIV and DES.
- The macro-scale analysis showed agreement between 4DPTV and TPIV for the SDVP elliptically shaped cross plane streamlines and Gaussian and Bell distribution for the axial vorticity and Q-criteria. The macro-scale turbulence is larger for the 4DPTV vs. the TPIV, whereas the vortex strength has the opposite trend, and the anisotropy shows both similarities and differences. The DES shows similar trends as the experiments, but there are large quantitative differences.
- The micro-scale analysis used model spectrums based on the 4DPTV and TPIV macro-scales, as benchmarks which were about half the size of their spatial resolutions and indicates that sub mm resolution is needed to accurately resolve the micro-scales.
- The Taylor micro-scales (λ_f) were consistently larger than their benchmarks and roughly twice their spatial resolutions. The larger λ_f resulted in the dissipation ε being significantly smaller than the benchmark. The η values were larger than the benchmark, but the difference with the benchmark were not as large as that for the λ_f .
- The 4DPTV resolves a larger portion of the inertial subrange with the Kolmogorov $-5/3$ slope, whereas the DES is only able to partially resolve the inertial sub range and then dissipates rapidly due to the lack of filter/grid resolution, as often exhibited in LES.

Conclusions and Future Research (2)

- The anisotropy analysis of the 4DPTV, TPIV, and DES showed similarities and distinct differences between the three results which highlights the strengths and limitations for characterizing the turbulence structure. The DES predicts an almost 2D turbulence state whereas the 4DPTV and TPIV display Reynolds stress ellipsoids that resemble oblate and prolate spheroids, respectively.
- The 4DPTV measurements and DES provide strong evidence that SDVP undergoes a spiral vortex breakdown/helical mode instability like KVLCC2 and 5415 at static drift $\beta = 30$ and 20 deg, respectively, and delta wings.
- Future research will focus on additional anisotropy analysis, including more points along a radial line perpendicular to the vortex core and along the vortex core upstream and downstream of $x/L = 0.12$, for a more global determination of the turbulence state and for evaluation of the eddy viscosity concept.
- FFT analysis is needed to determine the period and wavelength of the SDVP and SDVS vortex cores and the SDVS vortex shedding, and a triple-decomposition could be leveraged to remove the oscillation of the spiral vortex breakdown/helical mode instability for further temporal turbulence analysis.
- The interactions between SDVS and SDVP are complex, and future analysis will be done to determine the mechanism of the merging of SDVS and SDVP. To accomplish this, simultaneous and instantaneous vortex core tracking must be done for both SDVP and SDVS and distances between their cores must be evaluated over the entire measurement range and duration.
- TKE budget analysis needs to be done for both SDVP and SDVS for better understanding their progressions and interactions, which requires evaluation of the pressure transport term.

- Bernard, P.S., Turbulent Fluid Flow, John Wiley & Sons, Inc, 2019.
- Banerjee, S., Krahl, R., Durst F. and Zenger, C., “Presentation of Anisotropy Properties of Turbulence, Invariants versus Eigenvalue Approaches,” Journal of Turbulence, Vol.8(32), 2007, DOI:10.1080/14685240701506896
- Bhushan, S., Yoon, H., Stern, F., Guilmineau, E., Visonneau, M., Toxopeus, S., Simonsen, C., Aram, S., Kim, S.-E. and Grigoropoulos, G., “Assessment of CFD for Surface Combatant 5415 at Straight Ahead and Static Drift $\beta=20$ deg,” Journal of Fluids Engineering, Vol. 141(5), 2019, 051101.
- Bhushan, S., Yoon, H., and Stern, F., “Detached Eddy Simulations and Tomographic PIV Measurements of Flows over Surface Combatant 5415 at Straight-Ahead and Static Drift Conditions,” Ocean Engineering, [Vol. 238](#), 2021, 109658.
- Kang H. S., Chester S., Meneveau C., “Decaying Turbulence in an Active-Grid-Generated Flow and Comparisons with Large-Eddy Simulation,” Journal of Fluid Mechanics, Vol. 480, 2003, 129-160.
- Pope, S.B., Turbulent Flows, Cambridge Univ. Press, 2000.
- Sanada, Y., Starman, Z., Bhushan, S., and Stern, F., “Four-dimensional particle tracking velocimetry measurements of unsteady 3D vortex onset and progress for 5415 straight ahead, static drift and pure sway,” Physics of Fluids, Vol. 35(10), 2023, 105125.
<https://doi.org/10.1063/5.0165658>.
- Yoon, H. and Stern, F., “Phase-averaged TPIV Measurements for Surface Combatant 5415 in Pure Sway Maneuver: Experimental Setup, UA and Preliminary Results,” Proceedings of the 30th American Towing Tank Conference, Oct. 2017, Bethesda, MD, USA.

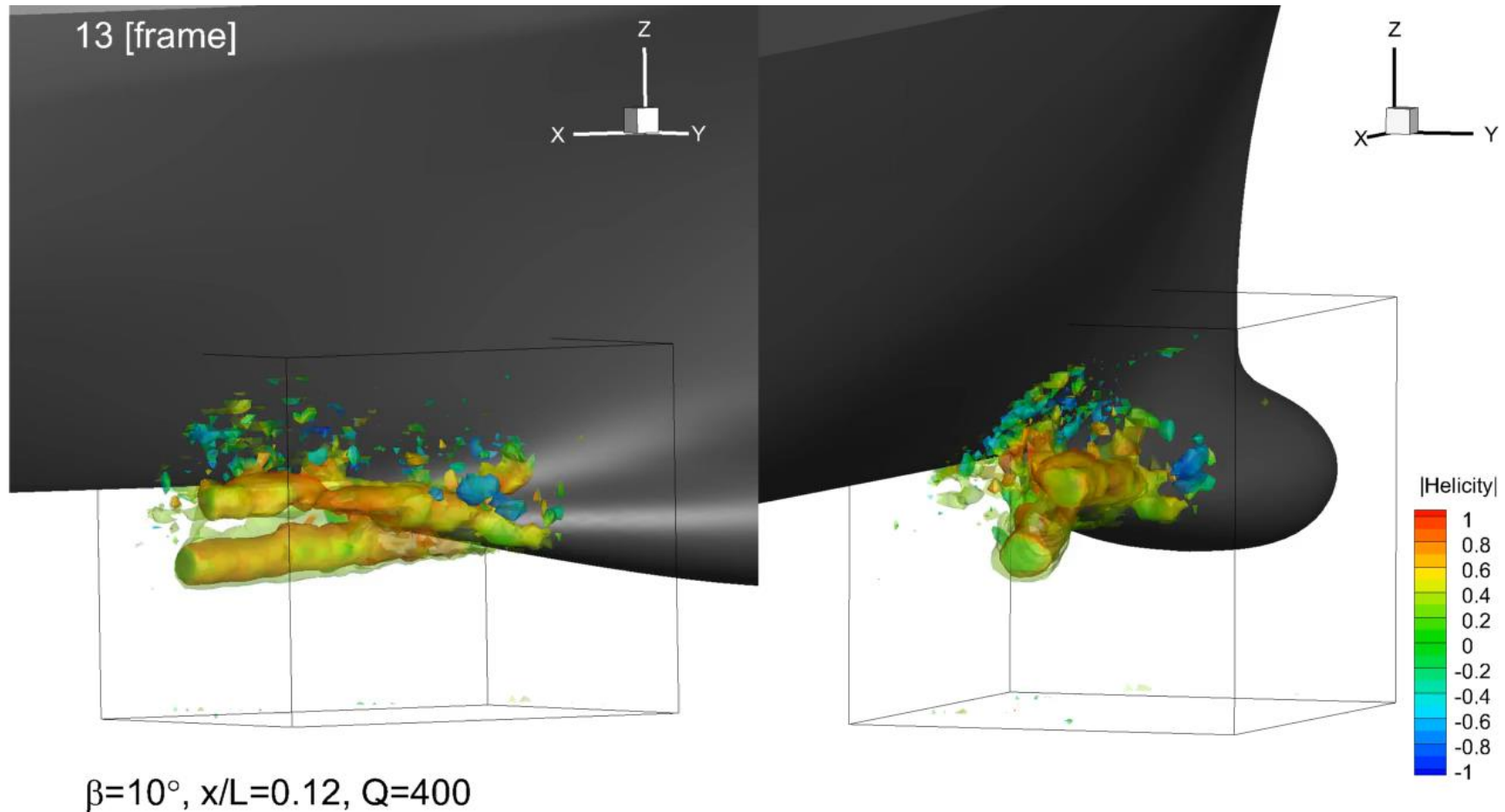
Introduction



Instantaneous vortex core analysis for static drift $\beta = 10$ deg.

[Return to slide 2](#)

Vortex Breakdown and Interaction (3)



Instantaneous Q isosurface colored with helicity ($\beta = 10$ deg).

[Return to slide 26](#)